2015

Constructing Morphometric Profiles along the Human Brain Cortex Using in vivo Magnetic Resonance Imaging (MRI)

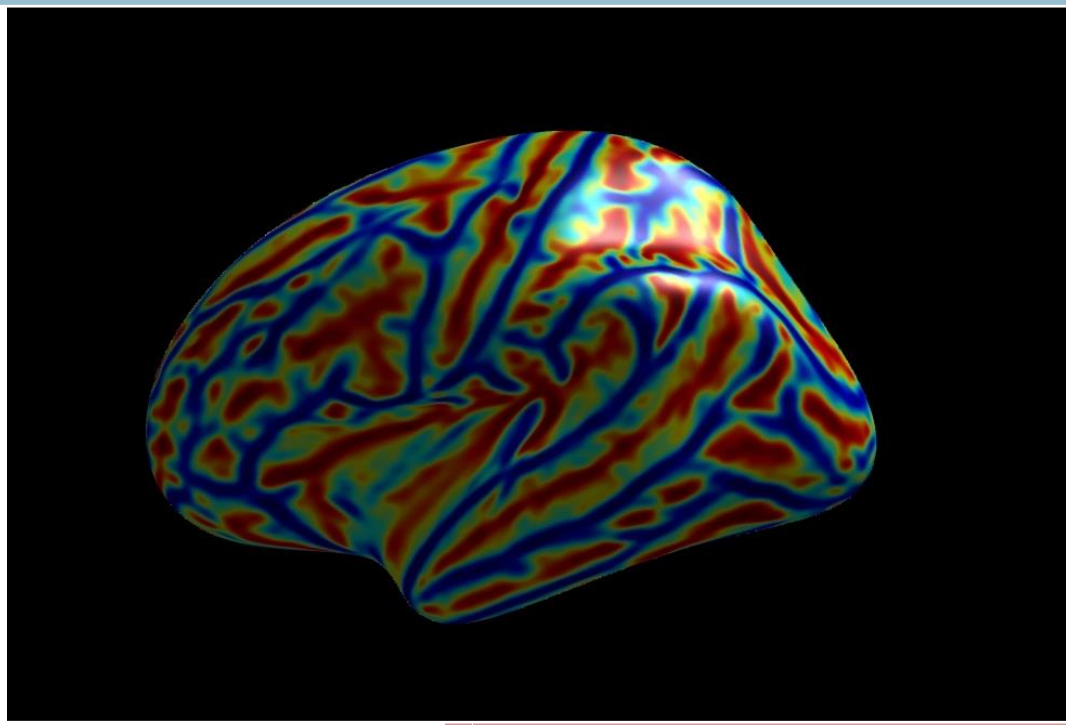

Author:

Javier Pérez Santonja

Tutor:

Manuel Desco Menéndez, MSEng, MD, PhD

Supervised by:

Manuel Desco Menéndez, MSEng, MD, PhD

Yasser Alemán Gómez, Eng, MsC

Universidad Carlos III de Madrid.

Departamento de Bioingeniería e Ingeniería Aeroespacial.

Universidad Carlos III de Madrid

www.uc3m.es

Summary

The geometry of the brain cortex is comprised of gyri (outward folds) and sulci (inward folds). Several biological properties about the anatomy and physiology of the brain cortex have been measured at the top of the sulci and at the bottom of the gyri; however, no one has yet measured how the values of these properties (called biomarkers) change along the path joining the top of the sulci and the bottom of the gyri. In this work, a methodology to display that information is shown, using different modalities of MRI images as input. There are four main steps to the methodology: the first two consist on obtaining the lines that run on top of the gyri and at the bottom of the sulci, while the next two make use of these lines to create a geodesic path between the top of the gyri and the bottom of the sulci and assigning biomarker values to each point of this geodesic path. The results of this work are composed of the validation of the methodology and three examples of possible applications of the methodology. These applications could be applied in future work to improve the detection and study the neurodevelopment of neurodegenerative diseases.

Contents

Chapter 1: General Introduction

1.1 Motivation

The human brain cortex presents an intricate geometry of ridges and grooves. This folding places the gray matter of the brain (cell bodies) in the outer surface, while keeping the white matter (axons and glial cells) below. In this geometry, *sulci* are defined as the regions of the cortex folded inwards ("valleys" or grooves) and *gyri* the regions folded outwards ("mountains" or ridges).

The development of medical image techniques, such as *magnetic resonance imaging* (MRI), has provided the researchers with a powerful tool to characterize and quantify, *in vivo*, different geometrical features of brain tissues in terms of shape, surface, depth or volume, increasing the knowledge of neurodevelopment and neuroimaging fields.

Along with medical image techniques, methods which convert the information within the images into quantitative biomarkers have also been developed. These groups of methods and algorithms are known as *brain morphometry techniques*. Biomarkers such as volume, cortical thickness or cortical gyrification can be mapped within the brain volume or on the brain cortex surface, providing an ideal framework to characterize their pattern over time and across individuals or groups.

The main drawback of these biomarkers lies on the impossibility for separating which part of its value corresponds to the sulci contribution and which to the gyri contribution. Several approaches for characterizing the brain cortex anatomy, separating both contributions, have been proposed. One of the most employed strategies is the study, independently, of sulcal fundi and gyral crests across the *sulcal lines* and *gyral crowns*.

The sulcal lines, which are commonly used to represent sulcal fundi, are mathematical objects running along the valleys of a cortical surface with maximum value of curvature within a sulcus. On the other hand, the gyral crowns, which are located on the top of the gyri, are the lines of maximum curvature within each gyrus.

The most important reasons to justify the study of sulcal lines and gyral crowns extraction are related to neurodevelopment due to the fact that cortex gyrification comprises an important biomarker when studying neurodevelopment, as seen in various

studies such as (Fischl et al. 2008; Melbourne et al. 2014). Also, other morphogenic and neurodevelopmental research proposes a tension-based theory about how the axonal bundles on the brain causes the cortex folding, showcasing the relevance of sulci and gyri in the brain's anatomical and physiological functionality (Essen 1997).

Because of the many applications in which sulcal lines are useful, the automatic extraction of sulcal lines has been an important objective for neuroscientists and researchers for over a decade. However, the automatic extraction of gyral crowns is an unexplored field in which almost no previous research can be found, since gyral crown applications are scarcer.

Knowing the exact location of the sulcal lines and gyral crowns it is possible to compute the geodesic lines that run across the cortical surface joining every gyral crown point to its closest points in the sulcal line. These paths are commonly called *sulcal depth paths* and a higher importance should be given to the longest depth path because it connects the gyral crown with the deepest point of the sulcal line, commonly called *"sulcal pit"*. These sulcal pits are related to intelligence and neurodevelopment in human brains (Im et al. 2011).

There are a large number of previous works on the study of biomarkers such as cortical thickness, gyrification index or curvature at the top of the crown, the bottom of the sulci and sulcal pits but none about how these biomarkers change across the depth path between gyral crowns and sulcal lines. For this reason, a new methodology, which calculates morphometric profiles to characterize and quantify how the biomarkers change along sulcal depth paths in the human brain cortex, is proposed.

To construct these morphometric profiles, four main steps must be performed: calculating the sulcal lines, calculating the gyral crowns, calculating the sulcal depth path and then projecting biomarkers values onto the points of the depth path. When calculating the sulcal lines, the previous methodology that has been published has certain disadvantages that made them unsuitable for this Project's requirements. In order to correctly overcome these disadvantages (more accuracy, more sensibility and faster computation time), a new method had to be developed. Gyral crown extraction methods also required many upgrades due to their primitive nature, and thus a whole new method

had to be developed. The other two steps in the construction of the morphometric profiles are a novel approach, and so there is no previous work on the matter.

The results stated as the main goal of this Project, which are composed of the possible applications obtained through morphometric profiles across the human brain cortex to study cortical and white matter biomarkers (obtained from T1W-MRI and DW-MRI, respectively), may provide useful information for the discussion of the aforementioned neurodevelopmental and morphometric research.

1.2 Socioeconomic Background for the Project

Due to the fact that the world's populations is aging, the number of people suffering from neurodegenerative diseases follows an exponential increasing trend (Brown et al. 2005). But not only the number of patients increases; the degree of the afflictions and the variety of diseases also grows. According to (Prince 2013), 35.6 million people lived with dementia worldwide in 2010, with numbers expected to double almost every 20 years.

The cost of caring for patients suffering from neurodegenerative diseases is also growing at a high velocity. A study portraying the direct costs of the caretaking of dementia patients (including treatment) in the U.S. in 2010 reported that between $159 billion and $215 billion were spent (Hurd et al. 2013). The same study also showcases the difference between these costs and those from conditions such as heart disease ($102 billion) and cancer ($77 billion).

With these figures in mind, it is clear that reducing these costs and preparing for the trend they will follow in the future is of utmost importance. The results generated in this work will provide some methodological framework for the study of the prevention of neurodegenerative diseases, which is one of the most difficult stages in their treatment. The possible applications that could be based on the research performed in this Project could also include clinical trials and essays, to be able to monitor how the patient is responding to different drugs in a reliable way. The costs of both the early detection and

the monitoring of the treatment are liable to decrease using the methodology in this work, as well as the number of affected patients and the degree of its disease.

1.3 Hypothesis and Objectives

Hypothesis

The construction of morphometric profiles using biomarkers will provide a more complete characterization and quantification of the human cerebral cortex anatomy.

Objectives

In this work two main objectives, which can be divided into several subgoals, have been set:

1. To obtain geodesic paths between gyral crowns and sulcal lines.
    a. To extract, in a robust way, both the gyral crowns and the sulcal lines.
    b. To compute the geodesic depth paths connecting the gyral crowns to the sulcal lines.
2. To compute morphometric profiles along the geodesic depth paths.
    a. To calculate different cortical biomarkers (cortical thickness and local gyrification index) from *T1-weighted* magnetic resonance images.
    b. To compute white matter biomarkers (fractional anisotropy, mean diffusivity and radial diffusivity) from *diffusion-weighted* magnetic resonance images.
    c. To project volumetric scalar maps containing values from biomarkers onto the cortical surfaces.
    d. To get biomarkers profiles across the geodesic paths.

1.4 Author's Contributions

These are the methodological tasks that the student presenting this report has performed for this Project:

- Bibliographical search on MRI and brain morphometry backgrounds, image processing pipelines and packages as well as previous work on sulcal lines and gyral crowns extraction (Chapter 2).
- Basic processing of neuroimages using software morphometry packages (FreeSurfer and BrainVisa) to work with cortical surfaces and morphometric biomarkers (Chapter 3.1 to 3.3)
- Optimization of the algorithms for sulcal lines extraction and gyral crowns extraction (Chapter 3.4 and Chapter 3.5).
- Design and implementation of algorithms for the geodesic profiles computation (Chapter 3.6 and Chapter 3.7).
- Validation of the sulcal lines extraction algorithm (Chapter 4.1) and description of some applications of the morphometric profiles (Chapter 4.2).

1.5 Budget

An estimation for the Project budget has been broken down in the following table:

Concept	***Number of subjects***	***Cost***	***Total(€)***
Image acquisition	165	300€/subject	49,500
Image processing and quantification	165	250€/subject	41,250
Personal	4 Person/month	1PM = 3,000€	12,000
Other goods and services			10,000
Total direct costs			112,750
Indirect costs (21%)			23,667
Total costs			136,427

1.6 Outline

This Project is divided in five chapters. The first chapter, **Chapter 1: General Introduction**, provides a brief motivation for the work, the general hypothesis and the

objectives to answer that hypothesis, the socioeconomic background of the Project and the listing of the author's contributions. The next chapter, **Chapter 2: Introduction and Previous Work**, includes some background in brain anatomy, MRI and brain morphometry so that the reader is able to follow the next chapters or refer to it when needed to. Also included in this chapter is a literature review about the state of the art on the extraction of sulcal lines and gyral crowns, some of the most important algorithms of the methodology of the Project. The next chapter, **Chapter 3: Methodology of Morphometric Profiles along the Human Brain Cortex**, contains the methodology of this Project, including the proposed methods for the extraction of sulcal lines and gyral crowns, the formation of the depth sulcal path and the construction of morphometric profiles, among other sections. **Chapter 4: Results and Discussion** presents the validation of the proposed methodology and the display of possible applications of the morphometric profiles. Finally, **Chapter 6: Conclusions and Future Work** introduces the conclusions of this Project, and also adds some comments on the limitations and future work. The last pages of this report include the **Related References**.

Chapter 2: Introduction and Previous Work

The brain cortex presents an intricate geometry of ridges and grooves. The biological utility of this structure is mainly based on the increased surface to total volume ratio that the folding causes. This is an advantage when it comes to keeping the size of the skull as small as possible to facilitate birth and at the same time increasing the cognitive abilities (Cusack 2005)**.** This folding also places the gray matter of the brain (cell bodies) in the outer surface, while keeping the white matter (axons and glial cells) below. The oxygen and glucose distribution by the circulatory system is more effective in this configuration because it reaches the cell bodies directly, since most arteries run through the surface of the cortex.

Sulci are defined as the regions of the cortex folded inwards ("valleys" or grooves) and *gyri* the regions folded outwards ("mountains" or ridges). In this model, the *sulcal lines* would be the "rivers" running through the sulci "valleys", while *gyral crowns* are the crests on top of the gyri "mountains" (see Figure 2.1). That is, a sulcal line corresponds to the line of maximum curvature within a sulcus, as a gyral crown comprises the line of maximum curvature within a gyrus. Sulcal depth is the geodesic line joining the gyral crown to the sulcal line and perpendicular to both.

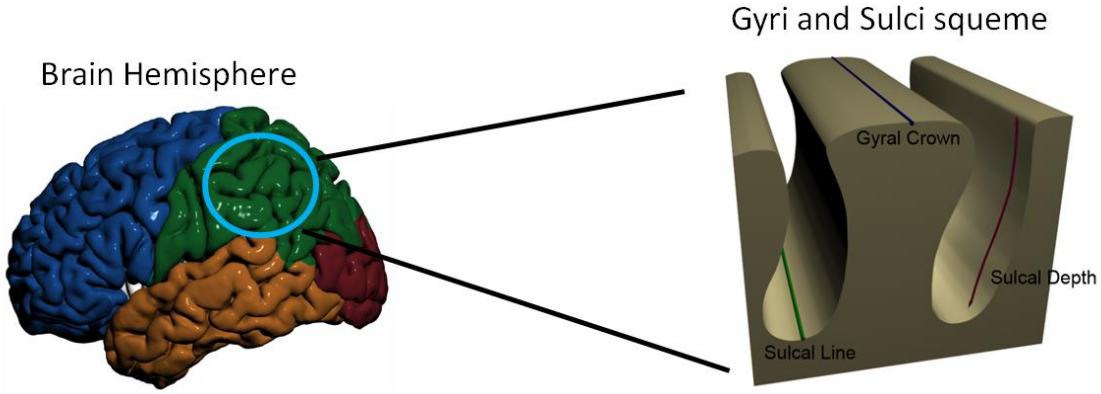

Figure 2.1: *Illustration of sulcal line, gyral crown and sulcal depth.*

Both sulci and gyri play an important role in the anatomy and physiology of the brain, since they are widely used as geographic landmarks for the segmentation of the cortex of each hemisphere into seven lobes. These lobes are the frontal, parietal, occipital, temporal, insular and limbic (Yaçargil 1996). Gyri and sulci are also very

relevant for neurosurgery; they can be used as guiding agents by neurosurgeons (Campero et al. 2014).

The most important reasons to justify the study of sulcal lines and gyral crowns extraction is related to neurodevelopment. The gyrification of the cortex comprises an important biomarker when studying neurodevelopment, as can be seen in various studies such as (Fischl et al. 2008; Melbourne et al. 2014). Also, other morphogenic and neurodevelopmental research, such as (Essen 1997), for example, propose theories on how the fiber tracts on the brain provoke the cortex's folding by tension-based methods, showcasing the relevance of sulci and gyri in the brain's anatomical and physiological functionality (see Figure 2.2).

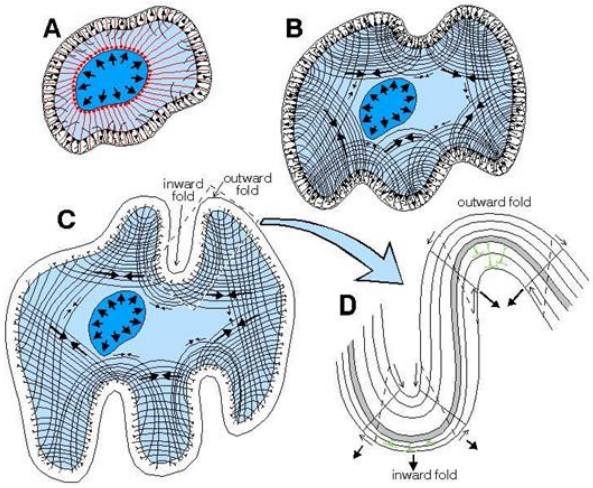

Figure 2.2: *Tension-based methods in brain development may be the reason for its intricate geometry of sulci and gyri. Image from (Essen 1997).*

The main goal of this Project, as stated in Chapter 1.3, is to obtain morphometric profiles joining the gyral crowns with the sulcal lines to study how some biomarkers change along the sulcal depth (from the top of the crown to the bottom of the sulci). In order to do that, sulcal lines and gyral crowns must be extracted from MRI images.

T1W-MRI images must be processed to form *cortical surfaces*, because extraction of sulcal lines and gyral crowns from cortical surfaces is easier and more reliable using surfaces (and the resolution is much higher). Since the sulcal lines and the gyral crowns are extracted from these surfaces, the rest of the algorithms used in this Project will also be performed using cortical surfaces.

This chapter presents some background on the MR images used in this work (T1W and DW), as well as on brain morphometry, which explains how cortical surfaces are obtained from T1W-MRI images. The different biomarkers used in this Project are also briefly explained, and finally, a bibliographical section about previous work done in sulcal lines and gyral crowns is displayed.

2.1. Brief Background on T1W-MRI and DW-MRI

Magnetic Resonance Imaging (MRI) is a tomographic image modality, whose main advantage relies on the fact that it is non-invasive and non-ionizing. In neuroanatomy, MRI has become the lead mapping tool due to its capacity to acquire 3D visualizations of neural structures *in vivo* with the highest spatial resolution of all image modalities.

There are many modalities of MRI used in neuroscience; the ones presented here are the ones used for this Project. They are *T1-Weighted MRI*, used for the extraction of cortical surfaces and cortical biomarkers, and *Diffusion-Weighted MRI*, used for the extraction of white matter biomarkers.

T1-Weighted MRI (T1W-MRI)

In anatomical MRI images, contrast depends on the different relaxation times of the tissues. There are two main types of relaxation times: these are called T1 and T2 (Liang et al. 2000). Both T1 and T2 vary depending on the tissue, and this variation constitutes the basis for the contrast in MRI. In the following figure the different contrasts obtained in two images pondered in T1 (Figure 2.3A) and T2 (Figure 2.3B) can be observed.

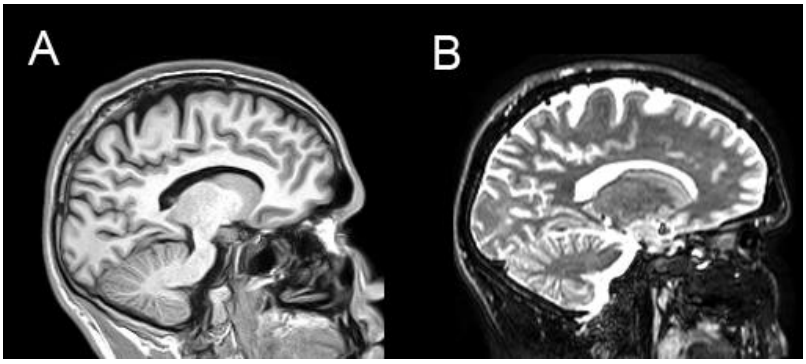

Figure 2.3: *MRI images.* ***A)*** *T1-Weighted image.* ***B)*** *T2-Weighted image.*

As the figure shows, *T1-Weighted images* (T1W-MRI) have darker intensities on the liquid components of the brain (like CSF, cerebrospinal fluid), and tend to be brighter on the more dense components, like fat tissue or white matter. *T2-Weighted images* (T2W-MRI) show darker intensities on white matter, while CSF and gray matter appear brighter. In this Project, only T1-Weighted images will be used.

Diffusion-Weighted MRI (DW-MRI)

Biological tissues can be divided into two main categories taking into account how the diffusion process takes place inside them: 1) *isotropic* tissues, where diffusion occurs with the same probability along any spatial orientation and 2) *anisotropic* tissues, where water molecules movement differs related to the spatial orientation. These diffusion differences might be due to the presence of obstacles or barriers which limit molecular movement or differences in intrinsic properties (permeability or viscosity) of the medium (Beaulieu 2002).

In the brain, white matter is a highly anisotropic tissue, mainly because the bundles of neuronal axons present in this tissue form impermeable fibers that direct the movement of water within them. This anisotropy allows *Diffusion Weighted Magnetic Resonance Imaging* (DW-MRI) for measuring and quantifying the underlying microarchitecture of biological tissues (Le Bihan 1995), using the the diffusion tensor ($\mathbf{D}$) (Basser et al. 1994) as a model for this quantification. In it, the anisotropy for each voxel is mathematically defined by a 3x3 symmetric and positive defined matrix.

Applying a singular value decomposition to this diffusion tensor matrix it is possible to obtain three main, orthogonal, diffusion directions ($\vec{v}_1, \vec{v}_2, \vec{v}_3$), given by its eigenvectors and the diffusivity value along each direction given by the corresponding eigenvalues ($\lambda_1, \lambda_2, \lambda_3$ assuming $\lambda_1, \geq \lambda_2 \geq \lambda_3$).

$$\mathbf{D} = \begin{pmatrix} \hat{D}_{xx} & \hat{D}_{xy} & \hat{D}_{xz} \\ \hat{D}_{yx} & \hat{D}_{yy} & \hat{D}_{yz} \\ \hat{D}_{zx} & \hat{D}_{zy} & \hat{D}_{zz} \end{pmatrix} = \begin{bmatrix} v_{1x} & v_{2x} & v_{3x} \\ v_{1y} & v_{2y} & v_{3y} \\ v_{1z} & v_{2z} & v_{3z} \end{bmatrix} \begin{bmatrix} \lambda_1 & 0 & 0 \\ 0 & \lambda_2 & 0 \\ 0 & 0 & \lambda_3 \end{bmatrix} \begin{bmatrix} v_{1x} & v_{2x} & v_{3x} \\ v_{1y} & v_{2y} & v_{3y} \\ v_{1z} & v_{2z} & v_{3z} \end{bmatrix}^T$$

2.1. Brief Background on Brain Morphometry

MRI techniques allow the detection of structural variations in the brain, and this knowledge can be used to either identify or exclude certain neuropathologies such as Alzheimer's disease, dementia or the degeneration of cognitive function. These structural variations consist mostly on the loss or atrophy of neural tissue, both of which can be identified using structural MRI sequences.

Traditionally, the analysis of the pathological inference in neural structure was performed by experimented radiologists and manual measurements of regions of interest (ROIs). However, these procedures are time-consuming and visually subjective, and its application to a large amount of patients exponentially increases the effort and the time length of the whole diagnostic process. That is the reason why automatic computerized methods have been developed during the last decade. Two of the most used methods are *Voxel Based Morphometry* (VBM) and *Surface Based Morphometry* (SBM). The methodology used in this Project works with surfaces (SBM).

These techniques require MRI images obtained through T1W-MRI and one of the most important steps is tissues segmentation. The tissues segmentation goal is to group the MR image voxels into clusters, named white matter tissue, gray matter tissue, cerebrospinal fluid and absence of brain tissue (Ashburner et al. 2000) (see Figure 2.4).

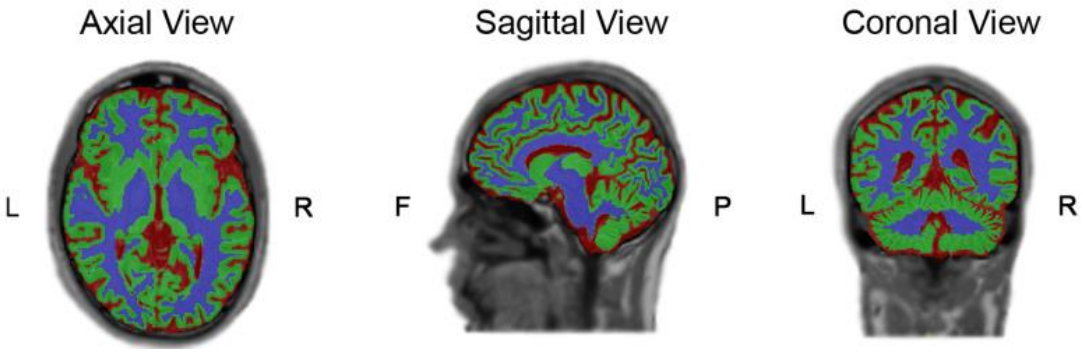

Figure 2.1: *Brain tissues segmented from T1-weighted images.* ***Red:*** *Cerebrospinal fluid.* ***Magenta:*** *White matter.* ***Green:*** *Gray matter.*

Once white matter (WM), gray matter (GM) and cerebrospinal fluid (CSF) volumes have been generated during the segmentation step, surface tessellations over gray/white and gray/CSF boundaries could be created. These tessellations yield *cortical*

surfaces (see Figure 2.5). Each cortical surface is modeled as a mesh formed by vertexes (X, Y and Z coordinates obtained during the surface extraction process from the images) and triangles known as surface faces (Davatzikos et al. 1996; Dale et al. 1999; Kim et al. 2005). The two types of cortical surfaces are the *pial surface* (obtained from the boundary of GM and CSF) and the *white surface* (obtained from the boundary between WM and GM).

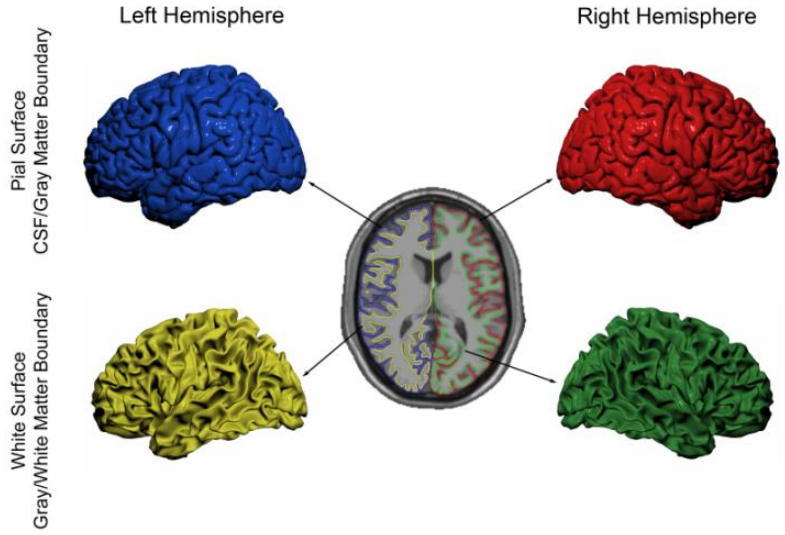

Figure 2.2: *Cortical surfaces (pial and white) extracted from T1W-MRI for both hemispheres.*

Other important surfaces that can be reconstructed are the *hull surface and the inflated surface* (see Figure 2.6). The hull surface is a smooth envelope that is wrapped around the pial surface but does not encroach into the sulci. On the other hand, the inflated surface is an auxiliary surface to show the areas inside the sulci for an improved visualization.

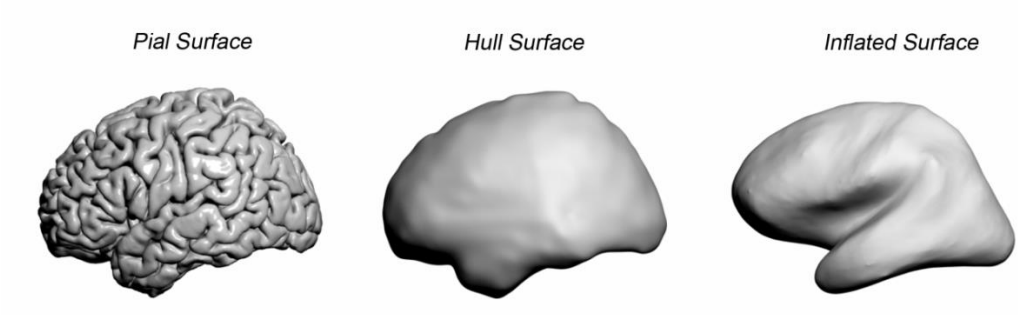

Figure 2.3: *Pial, hull and inflated surfaces extracted for a hemisphere.*

2.3 Morphometric Biomarkers

A biomarker is defined as "a characteristic that is objectively measured and evaluated as an indicator of normal biological processes, pathogenic processes, or pharmacologic responses to a therapeutic intervention" (2001). Within this context, a morphometric biomarker acts as a morphometric measure that can be studied across a population to analyze neurodevelopment or monitor neurodegenerative diseases. The main goal of this Project is precisely to create morphometric profiles that portray how some biomarkers change along the sulcal depth.

Several biomarkers obtained both from T1W-MRI and DW-MRI will be used in this Project. The ones obtained from T1W-MRI are *cortical biomarkers*, due to the fact that they are calculated from the cortical surfaces resulted from brain morphometry using T1W-MRI images. The biomarkers obtained from DW-MRI are referred to as *white matter biomarkers*, since they are calculated from the diffusion tensor and characterize how diffusion takes place inside white matter.

2.3.1 Cortical Biomarkers

Throughout the cortical surfaces, many global and local cortical morphometric measures could be obtained. However, only local measures were chosen to be used as biomarkers in this work. These are (see Figure 2.7):

***Cortical thickness** (CT):* CT corresponds, for a certain point, to the distance between the white surface and its corresponding point in the pial surface. It is a direct measure of the amount of gray matter contained in cortical layers along the perpendicular direction to each point on the surface.

Area: The area is calculated as the average of the areas of the three triangles to which a certain point belongs to in the cortical mesh.

***Local gyrification index** (LGI):* LGI quantifies the amount of cortex buried within the sulci folds as compared with the amount of cortex on the outer visible cortex in a given neighborhood around each surface vertex (Schaer et al. 2008).

Curvature map: The curvature map stores spatial information about gyral (convex) and sulcal (concave) regions over the cortical surface (Davatzikos et al. 2001). It is useful for describing which regions of the surface are concave and convex, and

thus, it provides significant geometrical information about the sulci and the gyri present in the surface.

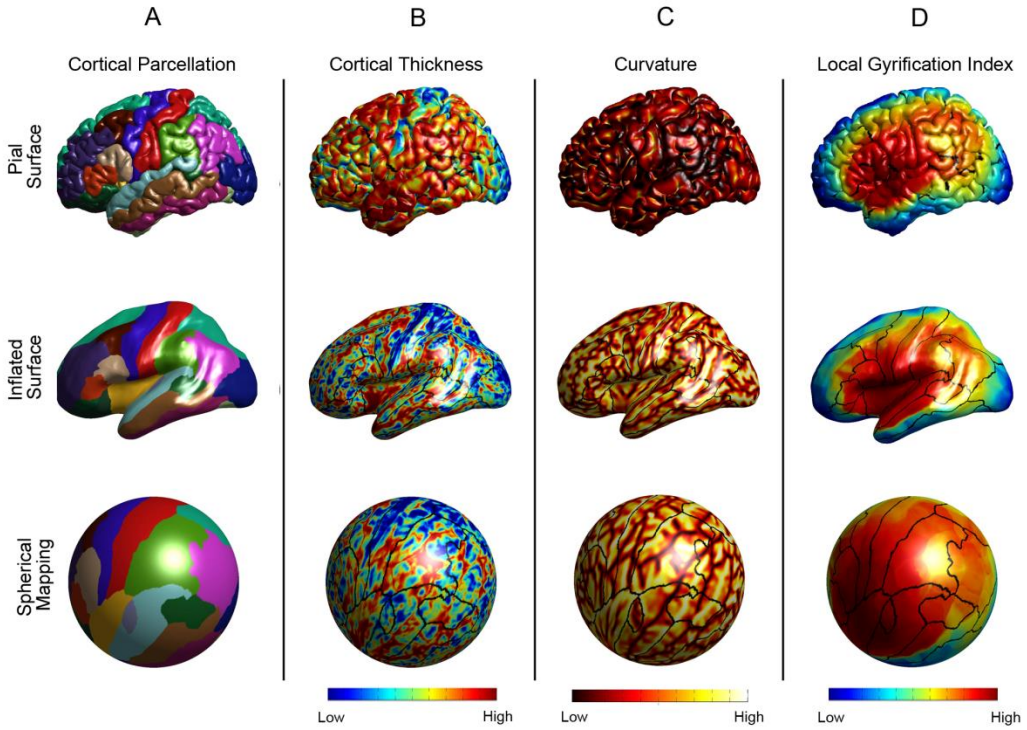

Figure 2.4: *Pial, inflated and sphere surfaces overlaid with cortical parcellation, cortical thickness (CT), curvature and local gyrification index (LGI) maps.* ***Note:*** *Inflated surface and spherical mapping are used to show the areas in the sulci.*

CT, LGI and Area will be used as biomarkers to be monitored along the sulcal depth with the aid of the morphometric profiles. However, the curvature maps will be used as a key input in the methodology of the sulcal lines and gyral crowns extraction and the construction of such profiles, as can be seen in Chapter 3.

2.3.2 White Matter Biomarkers

White matter biomarkers are extracted from the information obtained by Diffusion Weighted MRI. The diffusion tensor decomposition allows for computing several rotationally invariant scalar properties (biomarkers) which have been widely used to quantitatively characterize diffusion anisotropy (Basser et al. 1994; Basser 1995; Basser 1997). The ones used in this Project are (see Figure 2.8):

Fractional Anisotropy *(FA):* FA is the most commonly used anisotropy index and it measures the fraction of the diffusion that follows a certain direction (for example, if there are white matter tracts), relative to the amount of diffusion that does not follow a specific direction (if there is a low number of white matter tracts or if these tracts are perpendicularly located). FA measure is appropriately normalized so that it takes values from zero (isotropic diffusion) to one (anisotropic diffusion).

$$FA = \sqrt{\frac{3}{2}}\sqrt{\frac{\left(\lambda_1 - \bar{\lambda}\right)^2 + \left(\lambda_2 - \bar{\lambda}\right)^2 + \left(\lambda_3 - \bar{\lambda}\right)^2}{\lambda_1^2 + \lambda_2^2 + \lambda_3^2}}, \quad \bar{\lambda} = \frac{\lambda_1 + \lambda_2 + \lambda_3}{3}$$

Mean Diffusivity *(MD):* The mean diffusivity of the diffusion tensor is a measure of the overall diffusion in a voxel, independent of the gradient direction.

$$MD = \frac{\lambda_1 + \lambda_2 + \lambda_3}{3}$$

Radial Diffusivity *(RD):* Radial diffusivity is defined as the average of the two smallest eigenvalues of the diffusion tensor. This means that RD characterizes the two directions in which diffusion is lower.

$$RD = \frac{\lambda_2 + \lambda_3}{2}$$

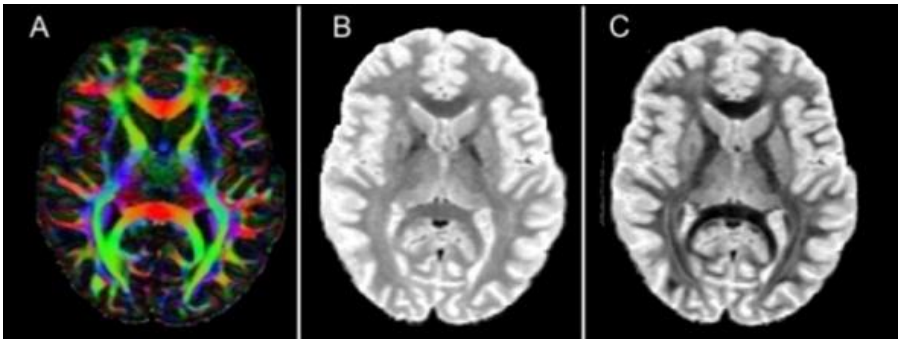

Figure 2.5: *Different scalar maps computed from diffusion tensor eigenvalues.* ***A)*** *Color coded fractional anisotropy. RGB (red-green-blue) color map indicates the major eigenvector orientation for each voxel.* ***Red****: Left-Right.* ***Green****: Anterior-Posterior.* ***Blue****: Inferior-Superior.* ***B)*** *Mean diffusivity.* ***C)*** *Radial diffusivity.*

2.4 Previous Work on Sulcal Lines and Gyral Crowns Extraction

The automatic extraction of sulcal lines has been an important objective for neuroscientists and researchers for over a decade. This is not only due to the specific properties which make certain sulcal lines a viable landmark for inter-subject image processing, ie. image registration (Durrleman et al. 2007), but also due to the potential applications of sulcal lines in various fields such as brain morphogenesis (Essen 1997), morphometry studies (Paus et al. 1996), neuroanatomy (Le Goualher et al. 1999), studies of neurological and cognitive features such as intelligence (Im et al. 2011), or pathology of neurodegenerative diseases, such as schizophrenia (Narr et al. 2000) or Alzheimer's (Thompson et al. 1998).

However, the automatic extraction of gyral crowns is an unexplored field in which almost no previous research can be found.

2.4.1 Sulcal Lines Extraction

A more official definition of sulcal lines, also called *sulcal fundi*, refers to them as the lines in which the curvature of their points is maximum within a sulcal region. A sulcal region is a surface of the cortex whose points have negative curvature due to their position inside inward-folded areas of the cortex; the boundary of the sulcal region corresponds to the imaginary boundary between the sulci and the gyri. Note that a sulcal line, therefore, would be the line whose points' curvature indexes, *in absolute value*, are maximum (all the points in the sulcal region have negative curvature).

Due to the geometry of the cortical surface, there are many separated sulcal regions in the brain, and this gives as a result the existence of many different sulcal lines. Different groups of neuroscientists, like (Ono et al. 1990) or (Joshi et al. 2010), have constructed atlases in which some major sulci are identified as common to all individuals, even though many of the smaller sulci differ between subjects.

However, extraction of sulcal lines does not have a *gold standard*, that is, the geometry of sulcal lines is not predefined in any case due to the variability between individuals. The method that is usually considered as *optimal* is the manual labelling by expert neuroscientists, used in many studies like (Li et al. 2010) or (Thompson et al. 1998), for example. This method is not automatic, though, and the intricate sulci three-dimensional geometry combined with the high but still limited resolution of the images

make it a very difficult and time-consuming job. It is clear that in order to assure accuracy of the process, reduce its length and standardize the final geometry of the sulcal line, an automatic or semi-automatic computational method is necessary.

A brief review of some of the methods proposed by different authors in the literature is presented below, to showcase the background and the improvements that the method developed in this Project needed to overcome.

Method #1: Dynamic Programming Generation of Curves on Brain Surfaces

In 1998, (Khaneja et al. 1998) developed a semi-automatic dynamic programming approach to generate curves on cortical surfaces; they used this software to obtain sulcal lines by manually selecting the start point and the end point of sulcal fundi, on which they implement a tracking method weighted by the curvature (see Figure 2.9).

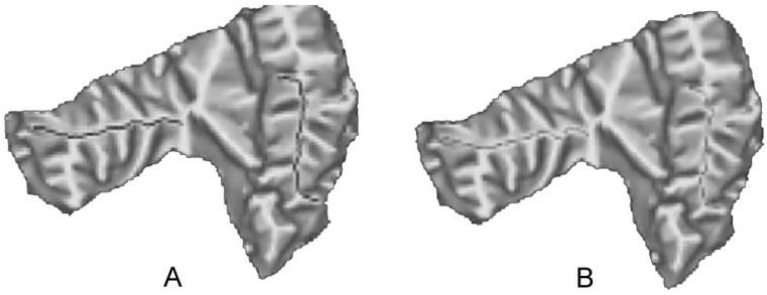

Figure 2.9: *Results from a surface-based semi-automatic sulcal lines extraction.* ***A)*** *Sulcal lines extracted by software.* ***B)*** *Sulcal lines drawn by expert, for comparison with the ones generated by software. Image from (Khaneja et al. 1998).*

Manually selecting the end points of the sulci is a problem to be found in many other approaches performed by different researchers, like (Le Goualher et al. 1999) and (Lui et al. 2006). This constitutes a problem for two reasons. Firstly, the automatization of the method is not full, and this increases the length and the tediousness of the process. Secondly, it may be an inevitable source of error, related to the imperfections manual labeling is prone to commit. The need for a whole automatic process turns out to be essential for fulfilling the problem's requirements.

Method #2: A Geometric Method for Automatic Extraction of Sulcal Fundi

In 2006, (Kao et al. 2007) proposed a method for sulcal fundi extraction in which they calculate all the depth paths between each pial surface point and the hull surface. Then, a threshold is applied to the depth map in order to obtain a skeleton of the sulcal basin which could be thinned and smoothed until the sulcal line is extracted (see Figure 2.10A).

Their results were validated by projecting their lines on to the manually labeled lines (drawn by a neuroanatomist) and using the distance between both lines as an error metric (see Figure 2.10B). Considering the possible human error of the neuroanatomist tracing the sulci, the results of the method can be considered as fairly good, but not optimal.

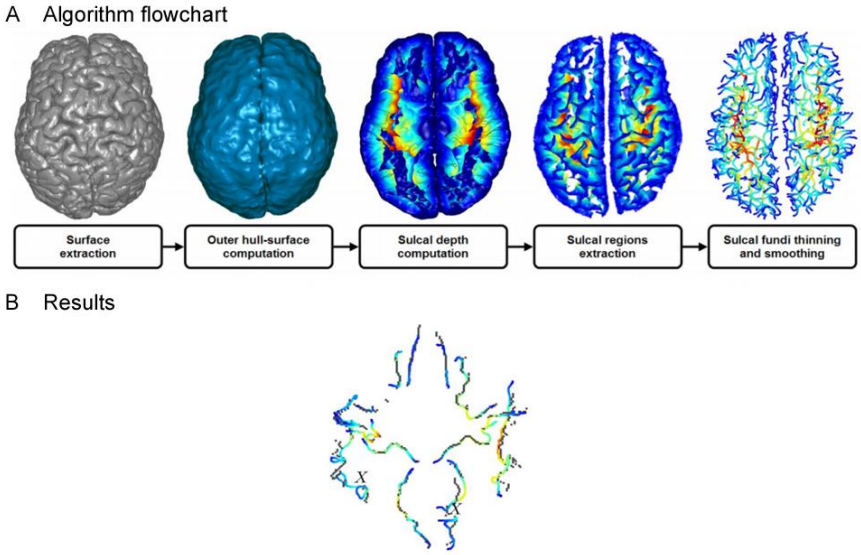

Figure 2.10: *Illustration for the method proposed by Kao et al.* ***A)*** *Overview of the process.* ***B)*** *Results of the algorithm (in color) compared to manual drawing (black dots). Image from (Kao et al. 2007).*

Method #3: Automatic sulcal line extraction on cortical surfaces using geodesic path density maps

Finally, in the method proposed by (Le Troter et al. 2012), a new biomarker, called the *Geodesic Path Density Map* (GPDM) was developed. This method is the one currently implemented in BrainVisa. The GPDM map is the superposition of all geodesic paths, calculated with Dijsktra's algorithm (Dijkstra 1959), between two

random points on the boundary of the sulcal basin. Thresholding the result with a histogram (the points which most paths cross have the highest values) gives the sulcal lines (see Figure 2.11).

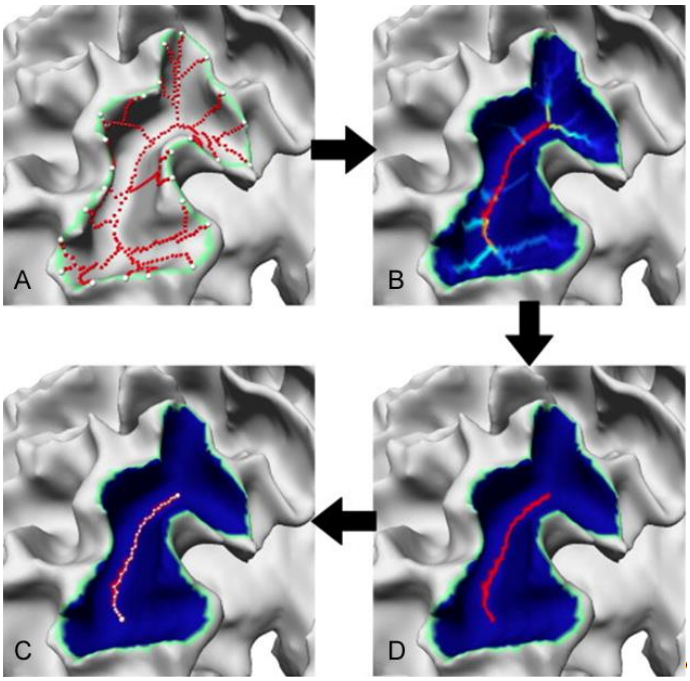

Figure 2.11: *Sulcal lines extraction for one sulcal basin using the* Geodesic Path Density Map. ***A)*** *A few geodesic paths between pairs of points on the boundary MRI.* ***B)*** *The resulting geodesic path density map.* ***C)*** *The thresholded GPDM.* ***D)*** *The final sulcal line. Image from (Le Troter et al. 2012).*

Two different metrics were employed to assess the method performance respect to a manual extraction approach: 1) the mean point-wise distances between the automatic extracted lines and the manual extracted ones and 2) the largest of the minimum distances between both lines (see Figure 2.12).

The results were also compared to the previous BrainVisa method. This method is a *snake-based* method, which is described in (Clouchoux et al. 2010). After the validation, they claim that their method works better than the snake-based and has low error when compared to the manual extraction. However, a large computation time (30 min per subject) is needed and a threshold, in order to obtain the final sulcal lines, must be selected.

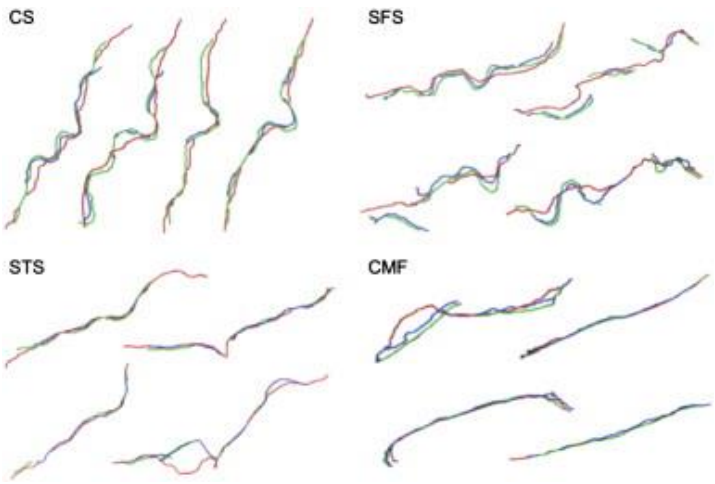

Figure 2.12*: Comparison of four major sulcal lines (CS = Central Sulcus, SFS = Superior Frontal Sulcus, STS = Superior Temporal Sulcus and CMF = Calloso-Marginal anterior Fissure) of four subjects between an expert's manual drawing (green), the snake-based method (red) and proposed GPDM algorithm (blue). Image from (Le Troter et al. 2012).*

In conclusion, it is easy to realize that a new sulcal lines extraction method based on cortical surfaces and curvature maps must improve the accuracy throughout the whole cortical surface (obtain small sulci as well as big landmark sulci) and reduce the computation time with respect to the previous work shown. Comparison with BrainVisa's Sulcal Fundi Extraction algorithm can be used as a validation resource, but keeping in mind that BrainVisa's algorithm is not optimal when compared to a manual labeling by an expert, and that this manual labeling may also have some errors due to the complicated and difficult geometry of the sulcal lines and the high but still limited resolution of the MR images.

2.4.2 Gyral Crowns Extraction

The objective of this work is not only limited to the extraction of the sulcal lines, but also to the automatic extraction of the gyral crowns (also called *gyral crests)*, the lines that form on top of the gyri and comprise the gyri points with maximum curvature.

The research performed on these lines is far scarcer than the research done on sulcal lines, possibly due to some of gyral crown's geometrical features, including the

fact that they are continuous through the brain cortex; that is, the gyral crowns form only one cyclic path. These features make it more difficult for the gyral crowns to be labeled, and therefore, to act as landmarks for inter-subject registration or for other anatomical and pathological studies, which comprised some of the main motivations for studying sulcal lines. Nevertheless, some previous background on the subject is shown.

Method #1: Marching Lines

In 1992, two computer scientists developed an algorithm for obtaining crest lines (Thirion et al. 1992), defined as the lines that contain the points which come from the intersection of two iso-surfaces (see Figure 2.13). This algorithm, which is called *Marching Lines*, comes from the *Marching Cubes* algorithm (Delibasis et al. 2001), which extracts iso-value surfaces (*iso-surfaces*) from 3D images. Obtaining two iso-surfaces and intersecting them will give the crest lines. The Marching Lines algorithm was applied to brain surfaces in 1993 (Thirion et al. 1993), showing promising results. However, no research on this algorithm was continued.

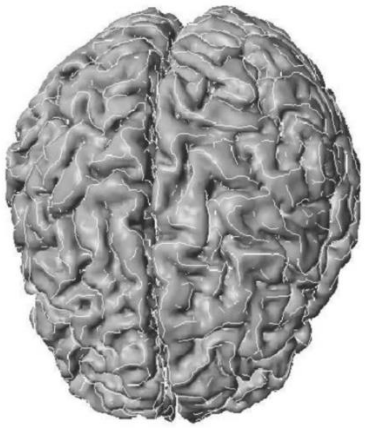

Figure 2.13: *Crest lines (gyral crowns) obtained with the Marching Lines algorithm. Image from (Thirion et al. 1993).*

Method #2: Depth level surface

A different approach is performed on (Lohmann 1998). In this paper, the outcome of the algorithm does not provide the real gyral crowns, but a good approximation can be obtained if some parameters are adjusted. The method uses

segmentation on a 3D MRI image to acquire the superposition of a white matter image with a depth level surface; this superposition can give an approximation of the gyral crowns if the depth is close enough to zero (see Figure 2.14). Also, this method incorporates what the researcher did in (Lohmann et al. 1997) to add sulcal lines into the results.

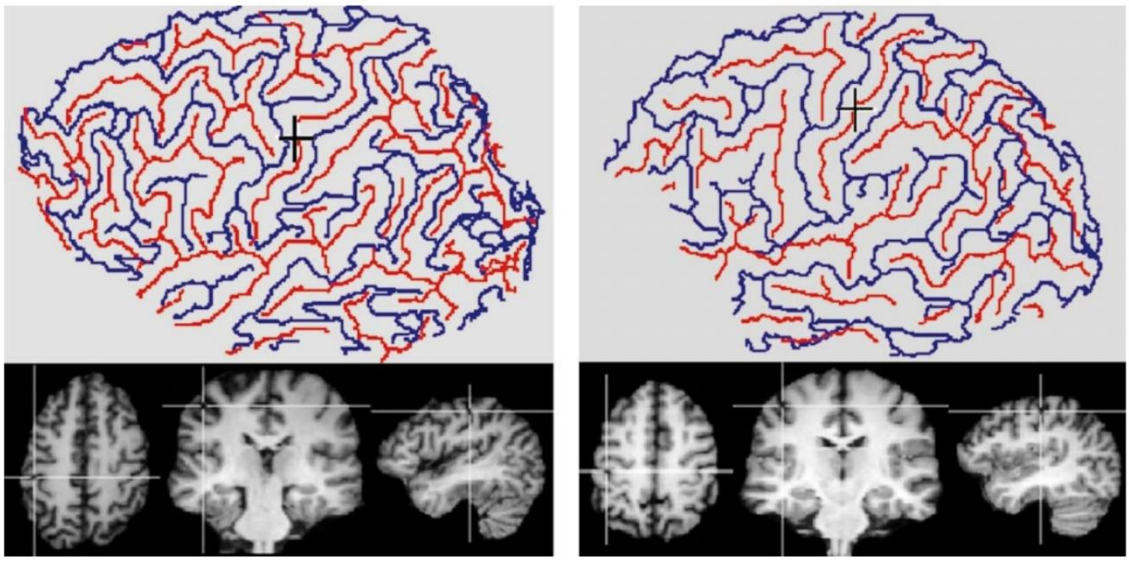

Figure 2.14: *Gyral crowns (blue) and sulcal lines (red) obtained by the superposition of a white matter image and a segmented 3D MRI with a depth level of 5 mm. Image from (Lohmann 1998).*

Both methods presented here are very old, however, and both work on 3D images rather than on cortical surfaces. The limited studies performed about the extraction of gyral crowns on meshes provides a very poor background on this problem, and thus there exists a big difficulty when it comes to validating the gyral crown extraction algorithm against another automatic algorithm.

Chapter 3: Methodology of Morphometric Profiles along the Human Brain Cortex

As it has been stated before, the main goal of this Project is to obtain morphometric profiles joining the gyral crowns with the sulcal lines in the human brain cortex. The reason why calculating the profiles is interesting is because many researchers have studied morphometric properties and biomarkers (both from MRI as from DW-MRI) at the top of the crown and at the bottom of the sulci, but no one has studied how these properties and biomarkers change across this path. The study of this gradient can provide with a deep understanding of cortex neurodevelopment, as explained in Chapter 1.1.

The methodology of this work can be divided in four main steps: calculating the sulcal lines, calculating the gyral crowns, calculating the sulcal depth paths and obtaining the profiles assigning biomarker values to the points of the depth path.

When calculating the sulcal lines, the previous methods explained in Chapter 2.4 had certain disadvantages that made them unsuitable for this Project's requirements. In order to correctly overcome these disadvantages, a new method had to be developed. This method should improve both the accuracy and the sensibility of the procedure, due to the fact that if some small sulcal line was not calculated or was geometrically misplaced, the correspondence with the closest gyral crown would produce artifacts and errors in the subsequent geodesic profile. Another feature that needed to be improved was the method computation time. The ultimate goal of this work is to analyze a large number of subjects, so the processing time for each subject must be reduced up to a minimum.

Gyral crown extraction methods also required many upgrades, and therefore, a whole new approach was taken. The main problem to solve was the fact that the new method must work on a surface mesh rather than a 3D image, so that it can be correlated with the sulcal lines.

A general workflow of the processes, including the new approaches for calculating sulcal lines, gyral crowns, geodesic depth paths and morphometric profiles is presented at Figure 3.1.

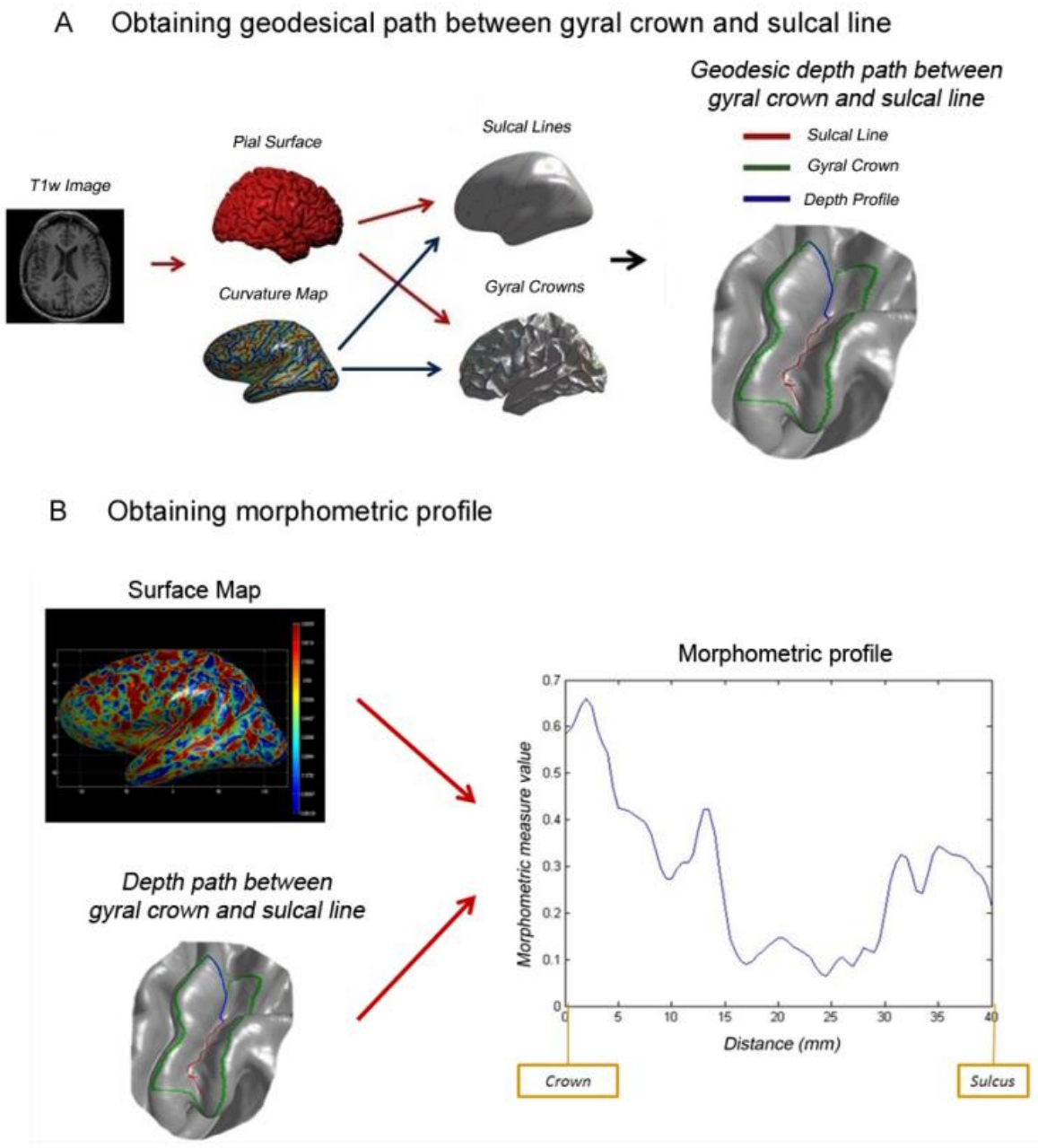

Figure 3.1: *Processing flowchart for the obtaining morphometric profiles along the human cortex.* ***A)*** *Obtaining superficial maps and a geodesical path from the gyral crown to the sulcal line from Diffusion-weighted MRI and T1-weighted MRI images.* ***B)*** *Obtaining a morphometric profile of a DW-MRI property (fractional anisotropy, in this example) from a superficial map and the geodesic path obtained in* ***A)***.

All computation processes will be executed on a 60 virtual machines cluster. Each virtual machine is compounded by a single core (2GHz or 2.6 GHZ) processor, 6 GB RAM and 50 GB of storage capacity. The image processing software packages used were Matlab (v2011), FreeSurfer (v5.1) and Brainvisa (v4.2.1).

3.1. Subjects Sample and Image Acquisition

A subset of 100 unrelated subjects (age range 26 – 31 years) were selected from the Human Connectome Project (HCP) database; sixty five of them contained also a follow up scan. These subjects were selected due to the high quality of the data, which will allow for an easier implementation of the designed procedures, although the full robustness of the experiments must be reassured (see Chapter 5.3).

All subjects were scanned on the same 3T Siemens Skyra platform with a 32 channels head coil at Washington University (WashU). The scanning protocol includes four imaging modalities: structural MRI, resting-state fMRI (rfMRI), task fMRI (tfMRI), and diffusion-weighted MRI (dwMRI) but only the T1W-MRI 3D MPRAGE and the DW-MRI were selected for all the participants. The scanning parameters for both MR sequences (T1 and DW) are shown at Figure 3.2.

For more details about the acquisition protocol see (Van Essen et al. 2012).

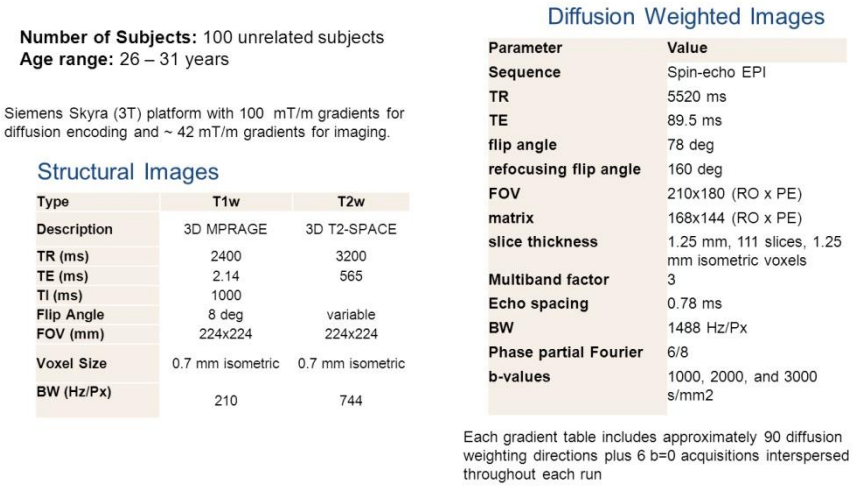

Number of Subjects: 100 unrelated subjects
Age range: 26 – 31 years

Siemens Skyra (3T) platform with 100 mT/m gradients for diffusion encoding and ~ 42 mT/m gradients for imaging.

Structural Images

Type	T1w	T2w
Description	3D MPRAGE	3D T2-SPACE
TR (ms)	2400	3200
TE (ms)	2.14	565
TI (ms)	1000	
Flip Angle	8 deg	variable
FOV (mm)	224x224	224x224
Voxel Size	0.7 mm isometric	0.7 mm isometric
BW (Hz/Px)	210	744

Diffusion Weighted Images

Parameter	Value
Sequence	Spin-echo EPI
TR	5520 ms
TE	89.5 ms
flip angle	78 deg
refocusing flip angle	160 deg
FOV	210x180 (RO x PE)
matrix	168x144 (RO x PE)
slice thickness	1.25 mm, 111 slices, 1.25 mm isometric voxels
Multiband factor	3
Echo spacing	0.78 ms
BW	1488 Hz/Px
Phase partial Fourier	6/8
b-values	1000, 2000, and 3000 s/mm2

Each gradient table includes approximately 90 diffusion weighting directions plus 6 b=0 acquisitions interspersed throughout each run

Figure 3.2: *Data and image acquisition specifications for the images used in this Project. These data was obtained from:* **http://humanconnectome.org/documentation/data-release/Q1_Release_Appendix_I.pdf**.

3.2. Image Processing

Brain mask extraction and intracranial volume assessment

Individual T1-weighted images were used to obtain brain tissues segmentation images using SPM8 (Wellcome Trust Centre for Neuroimaging, London, UK; available at: http://www.fil.ion.ucl.ac.uk/spm) (Ashburner et al. 2005). Subject's brain masks

were estimated using gray matter (GM), white matter (WM) and cerebrospinal fluid (CSF) segmentations throughout the VBM8 toolbox (available at: http://dbm.neuro.uni-jena.de/vbm)(Koutsouleris et al. 2012). The VBM8 algorithm produces a skull-stripped 'p0' image that consists of brain tissue classified into GM, WM, and CSF. The 'p0' images were binarized and visually inspected for correcting brain segmentation errors. Skull was manually removed if necessary. The skull-stripped T1 was obtained multiplying the native T1-weighted by the binarized brain mask. The intracranial volume (ICV) was defined as the number of voxels, in the binarized brain mask, that are different from 0 because of the voxel size is 1x1x1 mm^3.

FreeSurfer Processing

For each subject, the anatomical T1-weighted image was employed to estimate cortical thickness and gray matter regions using FreeSurfer package (version 4.5.3, http://surfer.nmr.mgh.harvard.edu). The white (WM/GM boundary) and pial (GM/CSF boundary) surfaces were reconstructed with the methods described by (Fischl et al. 1999; Fischl et al. 2002). Cortical thickness, local gyrification indexes and area and curvature maps for global brain were computed from white and pial surfaces.

Diffusion weighted images processing

For each subject, diffusion tensors fittings were performed using the FMRIB's diffusion toolbox (FDT, http://fsl.fmrib.ox.ac.uk/fsl/fslwiki/FDT/) (Smith et al. 2004). Afterwards, diffusion tensors eigenvalues were used to compute several scalar maps: fractional anisotropy (*FA*), mean diffusivity (*MD*) and radial diffusivity (*RD*) (Basser et al. 1994; Basser 1995).

3.3. Sulcal Basins Segmentation

The first step on both sulcal lines and gyral crowns extraction corresponds to the creation of the sulcal basins. The sulcal basins are the regions of the surfaces that contain a single sulcal line; its boundary corresponds to the imaginary line between the sulci and the gyri, and, therefore, the points that form a sulcal basin will all have a negative curvature index (concave region, according to the FreeSurfer curvature

estimation procedure, see Figure). Hence, to obtain these sulcal basins a curvature map must be used.

The curvature map is obtained from the white surface, as described in the previous section (Chapter 2.3.1 and Chapter 3.2). To obtain the sulcal basins, the curvature map was thresholded using a curvature threshold equal to zero in order to keep only the points with negative curvature (points of the sulcal basin). This threshold level was fixed to zero, assuming that points with curvature equal to zero are inflection points where the grooves start to become cortical gyri and vice versa. The result of this thresholding is a surface with the convex regions of positive curvature on one side and the concave regions of negative curvature on the other (see Figure 3.3A).

Finally, using a region-growing algorithm, each sulcal basin is adequately labeled. This labelling allows for a quicker processing of the whole surface by doing one sulcal basin at a time when calculating the sulcal lines, and it also will be crucial for the extraction of the gyral crowns and the geodesic depth paths (see Figure 3.3B).

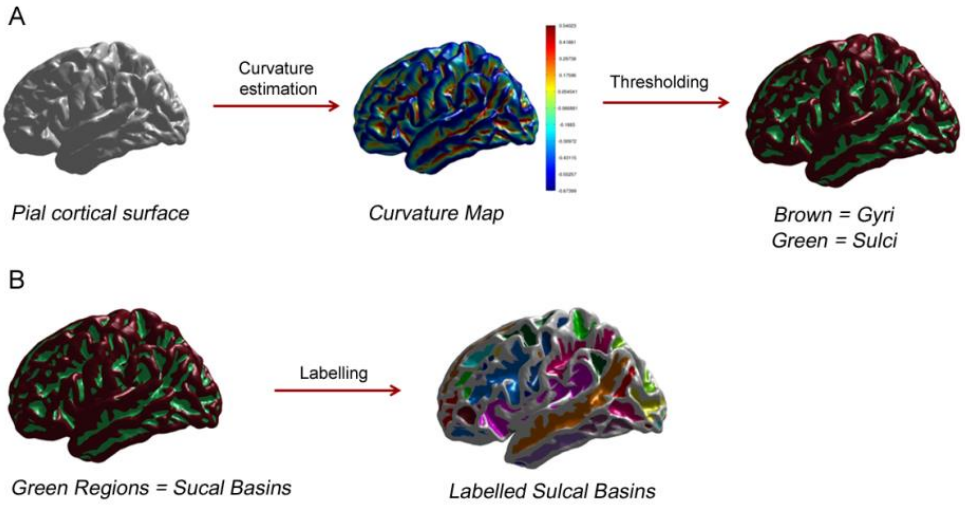

Figure 3.3: *Obtaining sulcal basins.* ***A)*** *Thresholding the curvature map with a curvature threshold of 0 separates convex (brown) and concave (green) regions, the latter being sulcal basins.* ***B)*** *Labelling of the thresholded surface gives the sulcal basins, each with a different value.*

3.4. Proposed Method for Sulcal Lines Extraction

The proposed method for the extraction of sulcal lines involves two main stages: 1) creating a graph for each sulcal basin surface and 2) computing the sulcal basin line throughout a skeletonization method applied to each sulcal basin graph. Using this approach it is not necessary to fix any threshold to define the sulcal line, like in (Le

Troter et al. 2012), or to select a priori the sulcal line endpoints, like in (Khaneja et al. 1998). This implementation is fully automatic and free of parameter selection.

3.4.1. Creating the Sulcal Basin Graph

In the first stage, a graph is constructed from the sulcal basin surface (see Figure 3.3B). Each sulcal basin triangular mesh can be represented as a non-directed weighted graph $G_{basin} = (N, E, W)$, where N is the set of *nodes* (surface vertices), E is the set of connections between pairs of contiguous surface vertices, commonly called *edges* and W is a set of real numbers representing *edges weights* (connection strength between edges endpoints). The weight of an edge is chosen according to the curvature values of its endpoints and, in this work, it was defined as the inverse of the mean edge endpoints curvature. Therefore, the mathematical expression for the edge weight w_{ij} between vertices i and j is:

$$w_{ij} = \frac{2}{C_{vi} + C_{vj}}$$

where C_{vi} and C_{vj} are the curvature values for the vertices i and j respectively. See (Shattuck et al. 2009) for a more extensive description of the graph method.

This weight definition allows for finding the path, between any two graph nodes, that minimizes the sum of weights along its edges using the Dijkstra's algorithm (Dijkstra 1959).

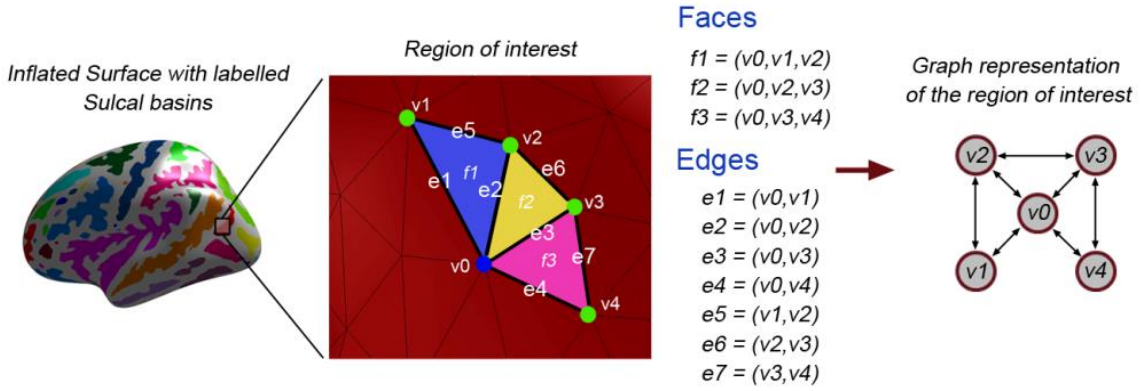

Figure 3.4: *Graph representation of a region of interest inside a sulcal basin compounded by five vertices and three faces.*

The main advantage of using a graph representation of the sulcal basin surface is that it allows using all the properties, measures and algorithms that have been developed by the graph theory in order to characterize graphs structure and organization. One of the most employed indices in graphs characterization is the *node degree* (or *valency*). The node degree is the number of edges incident to a specific node and it allows for dividing the graph nodes into four main categories:

- *Isolated node*: A vertex with degree equal to zero is a vertex that is not an endpoint of any edge.
- *Leaf node* (also *pendant vertex*)**:** A vertex with degree equal to one. The sulcal line is a path (sequence of edges) connecting two leaves nodes.
- *Path node*: A vertex with degree equal to two means that this node is in the middle of a path between leaves or junction nodes.
- *Junction node*: A junction node (degree higher than two) is a vertex where two or more paths coming from leaves vertices intercept.

3.4.2. Computing the Sulcal Basin Skeleton

Once we have the weighted graph, created for each sulcal basin (see Figure 3.5), the skeletonization process begins. This approach is based on a topological method used for obtaining terrain skeleton lines, which can be seen in (Gülgen et al. 2004).

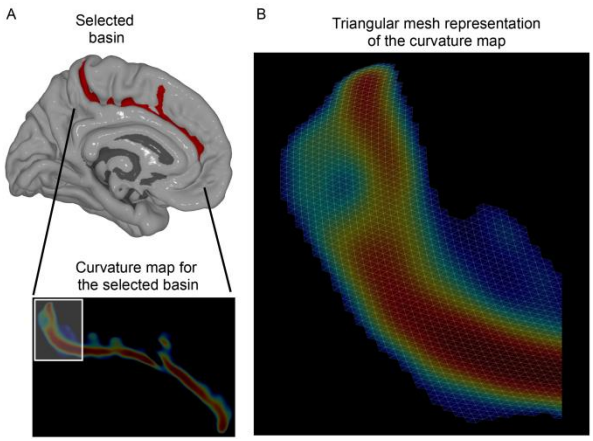

Figure 3.5: ***A)*** *Selected sulcal basin and its corresponding curvature map.* ***B)*** *Triangular graph representation of a sulcal basin mesh surface.*

The first step of the process, called *polygon breaking* (Figure 3.6), is a procedure to eliminate the edge with the highest weight from each graph polygon (surface face). None of the edges belonging to the sulcal line will be removed during this step because of the sulcal line is compounded by edges with the lower weight of their respective graph polygons (surface triangles).

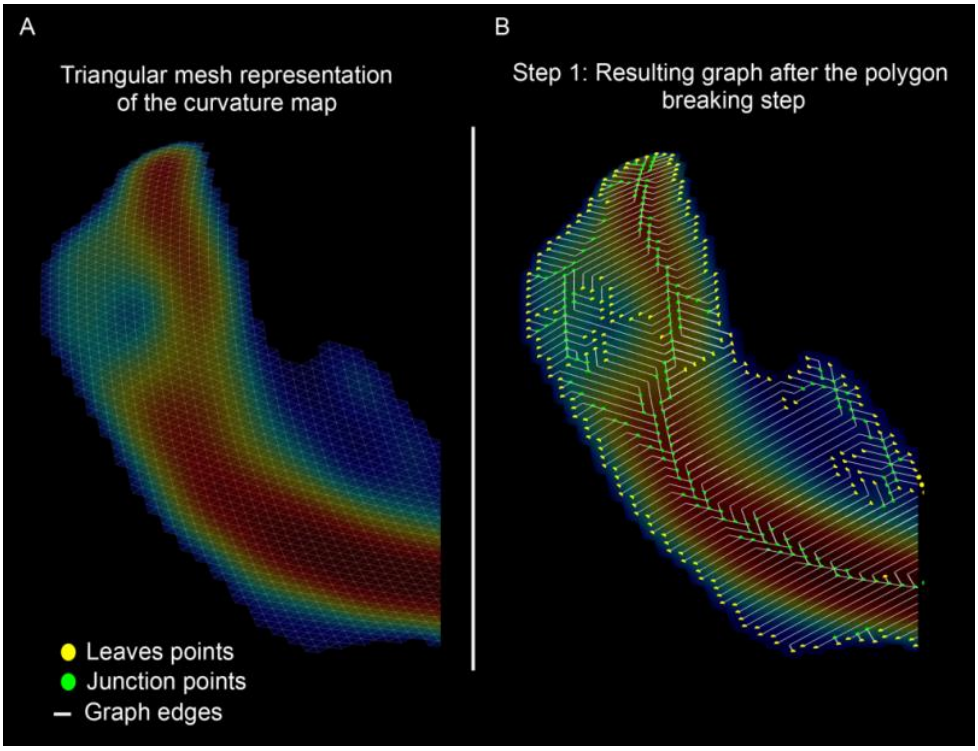

Figure 3.6: *Sulcal basin graph.* ***A)*** *Original graph. All surface points are considered as graph endpoints.* ***B)*** *In white are represented the remaining graph edges (and its corresponding endpoints) after the polygon breaking step. Leaves and junction points are represented in yellow and green respectively.*

This step allows the graph structure to transition from a *polygon-shaped* graph (see Figure 3.6A) to a structure quite similar to *tree-shaped* graph (see Figure 3.6B), but with cycles.

A tree graph is an undirected graph in which any two nodes are connected by exactly one path. Any connected graph without simple cycles is a tree. The interest of converting the graph into a tree-shaped graph lies in the analogy of these structures with the problem that has been set. In this case, the sulcal line would be the trunk of the tree and the pathways leading to the trunk would be the branches of the tree. For this reason, the next processing step is to convert the remaining graph into a tree-shaped graph. To achieve this aim it is necessary to remove any graph cycles from its structure computing its corresponding spanning tree graph.

A spanning tree of a connected graph ***G*** can be defined as a maximal set of edges of ***G*** that contains no cycle, or as a minimal set of edges that connect all vertices (Prim 1957). The employed algorithm to obtain the spanning tree is the algorithm proposed by (Kruskal 1956), which is implemented in the MATLAB function "*graphminspantree*" (http://es.mathworks.com/help/bioinfo/ref/graphminspantree.html). A graph and its corresponding spanning tree are shown at Figure 3.7.

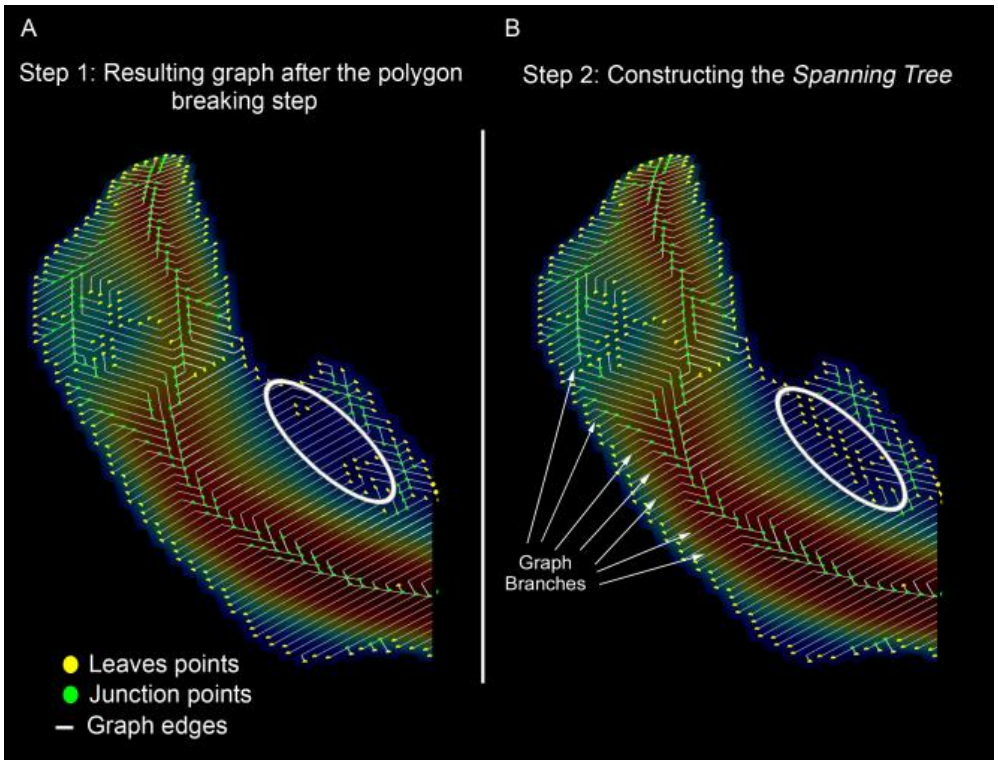

Figure 3.7: ***A)*** *Sulcus graph after the polygon breaking step.* ***B)*** *Corresponding spanning tree graph.*

Once we have obtained a tree-shaped graph, an iterative process, called *branch reduction*, is applied. The branch reduction step is the most important step, since it is responsible for obtaining the *sulcal basin skeleton* by eliminating edges from the graph structure.

In this work a branch will be defined as the shortest path between a leaf node and its closest junction or leaf node. A branch path can be defined by the sequence of nodes or edges that conforms the branch path.

The representation using the graph nodes can be mathematically stated by:

$$\beta_v = v_1, v_2, v_3, \ldots, v_n$$

where v_1 is always a leaf node, v_n can be either a leaf or a junction node and nodes from $v_2, v_3, ..., v_{n-1}$ can be neither leaves or junction points.

The mathematical definition using the graph edges can be expressed by:

$$\beta_e = e_1, e_2, e_3, ..., e_{n-1}$$

where v_i and v_{i+1} are ith and the ith+1 endpoints respectively of the ith edge e_i.

In the branch reduction algorithm, a branch is removed from the graph if and only if, along the entire branch path, the edge weight gradient (weight differences between all adjacent edges) is either an entirely increasing or decreasing monotonic function.

$$\nabla w_e = (w_{e1} - w_{e2}), (w_{e2} - w_{e3}), ..., (w_{en-2} - w_{en-1})$$

where $(w_{ei} - w_{ei+1})$ is the weight gradient between the ith and the ith+1 edges respectively.

As it was mentioned before, the branch removing step is an iterative procedure and it is repeated until there are no more branches whose weights gradient is a monotonic function. The result from the branch removing step is the sulcal basin skeleton graph (see Figure 3.8A and B).

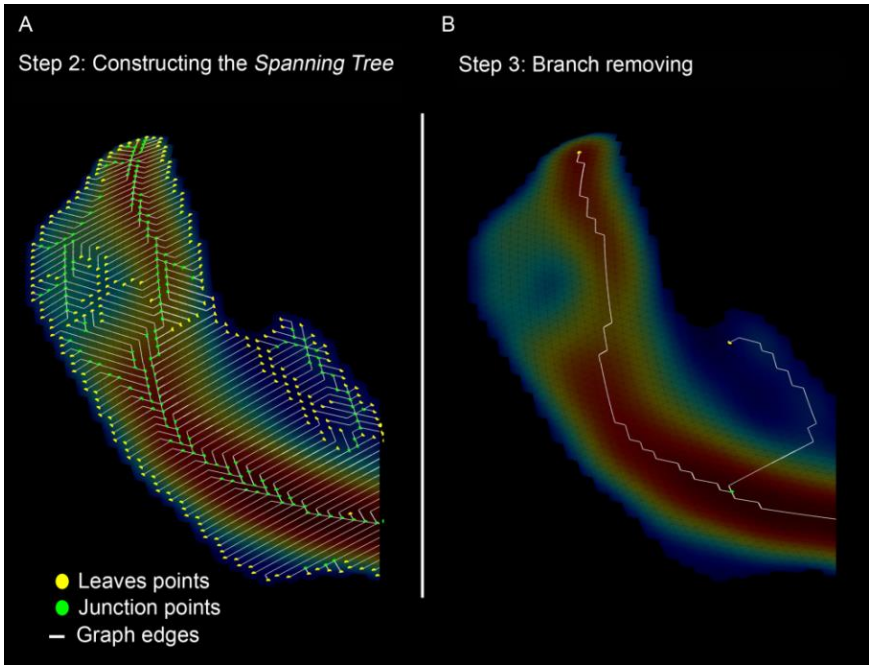

Figure 3.8: ***A)*** *Sulcal basin spanning tree graph.* ***B)*** *Results after the branch reduction step.*

The last step consists on the sulcal line extraction from the skeleton graph. To obtain the sulcal line the Dijkstra algorithm is employed to obtain the edge paths between every pair of the remaining leaf nodes. From all the possible pathways, the path that accumulates the highest weight value along the whole trajectory will be chosen as the sulcal line and the leaf nodes connected by this path will be the sulcal line endpoints (see Figure 3.9).

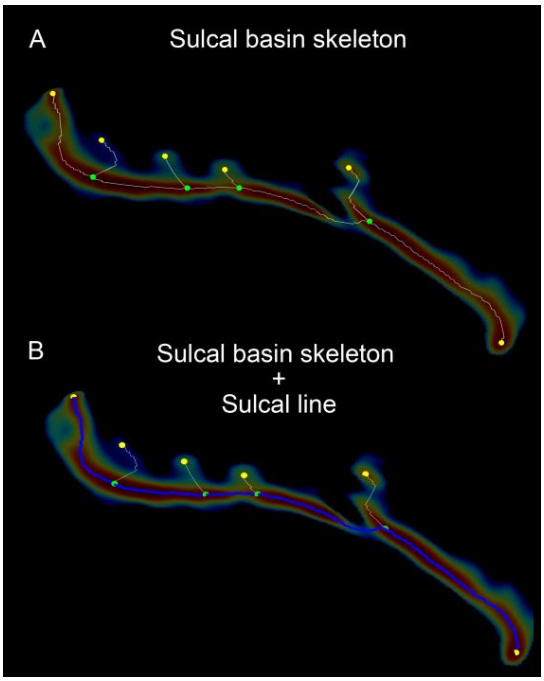

Figure 3.9: ***A)*** *Sulcal basin skeleton.* ***B)*** *Sulcal line (blue) over the sulcal basin skeleton. Leaves points (yellow) and junction points (green) are also represented.*

If the procedure described during this section is applied to each sulcal basin, the results are the sulcal lines for the whole brain (see Figure 3.10 and Figure 3.11).

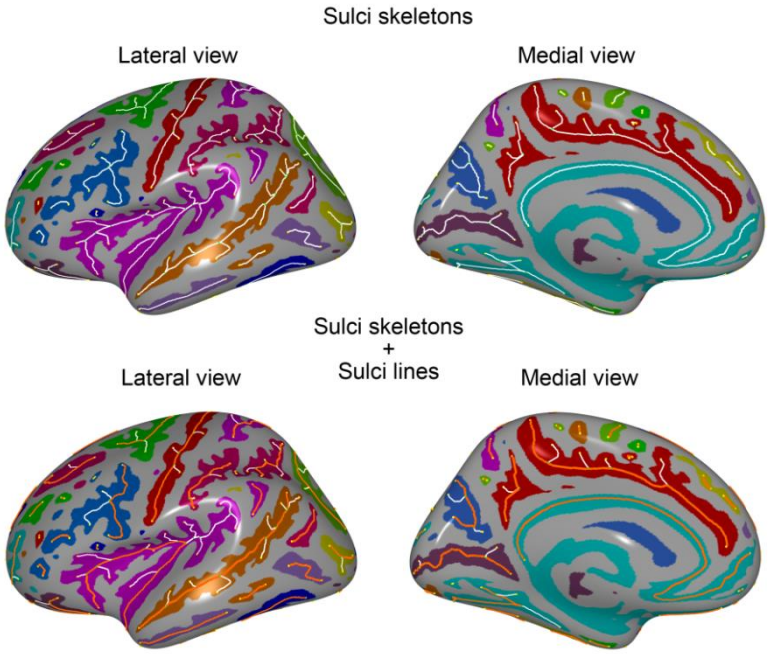

Figure 3.10: *Sulci skeletons and sulcal lines (**orange**) overlaid over sulcal basins.*

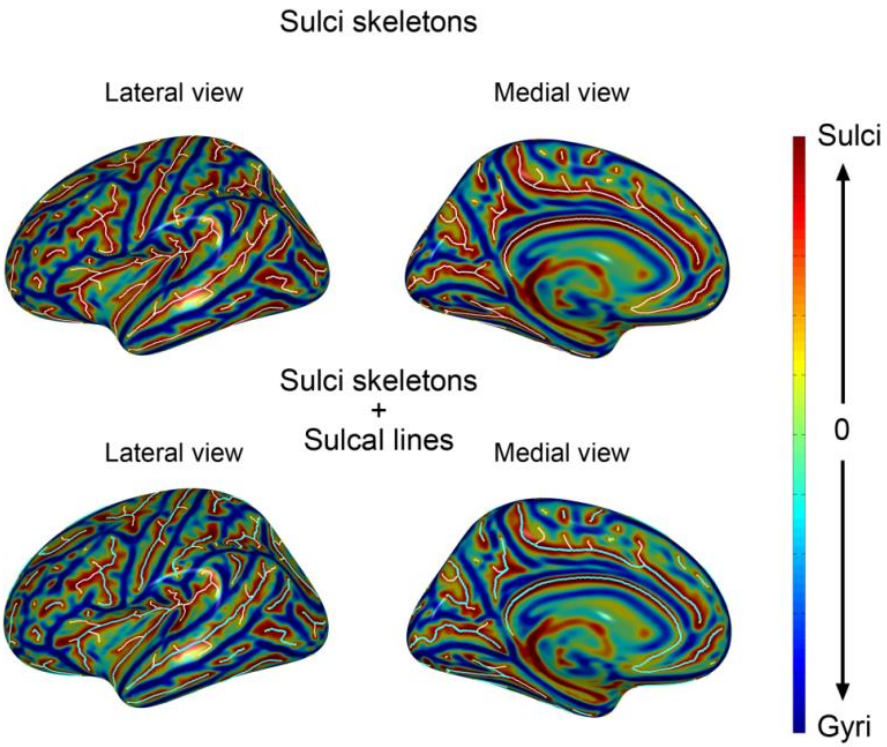

Figure 3.11: *Sulci skeletons and sulcal lines (blue) overlaid over the curvature map.*

3.5. Proposed Method for Gyral Crowns Extraction

The proposed method for gyral crowns extraction is based on a watershed method restricted by the curvature values of the surface points.

The main idea of the watershed algorithm is metaphorically based on two adjacent vessels on which water is poured (see Figure 3.12A). The line at which the water from one vessel meets the water from the other is the boundary between vessels (see Figure 3.12B). A graphical example can be seen in the next figure:

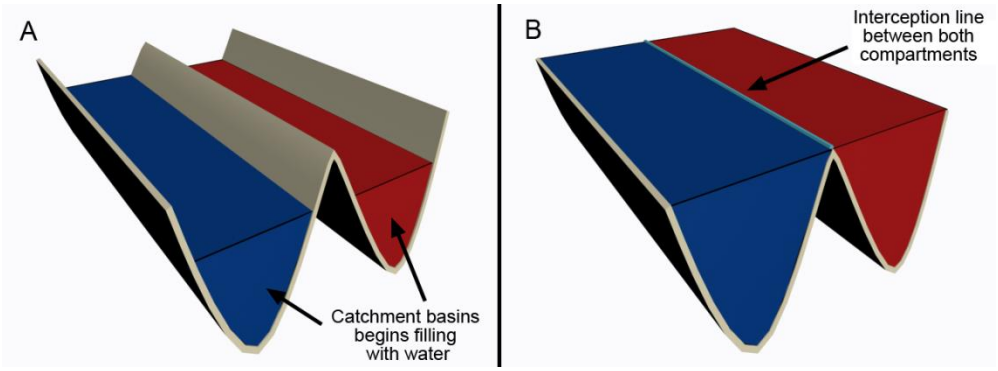

Figure 3.12: *Schematic figure portraying how the watershed algorithm can be used to obtain the gyral crowns.* ***A)*** *Watershed algorithm initialization. Both compartments contain water.* ***B)*** *The interception line between the water from both compartments will be the gyral crown.*

The application to gyral crowns extraction is inferred from this example The inputs are the sulcal basins that come out from Chapter 3.3, in which the cortical surface is divided into convex regions (gyri regions) and concave regions (labeled sulci regions). Watershed techniques on cortical surfaces have been explored before, for example, in (Rettmann et al. 2002); however, they have not been used to calculate gyral crowns, so it can be considered as a novel approach.

First, the curvature values of the sulcal basins boundary points are compared to the curvature of its unlabeled neighbors (see Figure 3.13B *(blue dots)*). If the curvature of it unlabeled neighbors is higher than the curvature values of the labeled points, i.e. Figure 3.13C *(green dot)*, the boundary is moved to these neighboring points (Figure 3.13D). In the case than the labeled neighbor points belong to different sulcal basins the growing point will be labeled with the tag present on the largest number of neighbors.

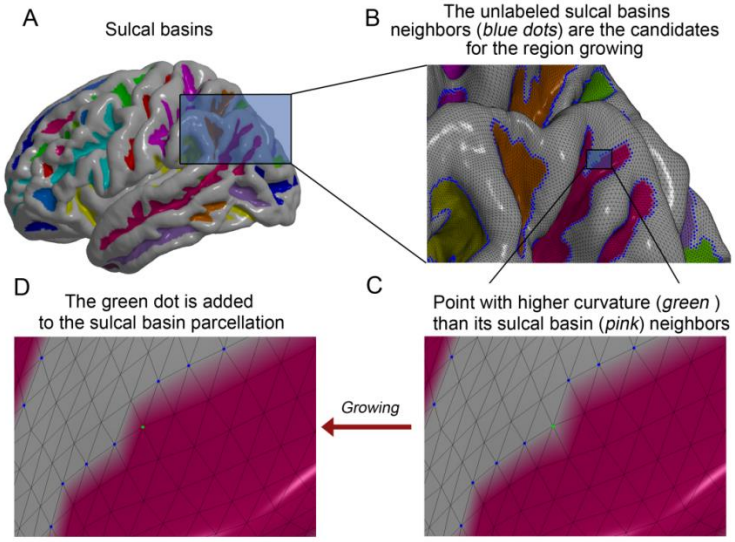

Figure 3.13: *Sulcal basins grow during the curvature restricted watershed procedure.*

This procedure is repeated until every surface point is labeled. During this iterative process, each sulcal basins boundary grows only until the gyri maximum curvature points are reached due to the growth being curvature restricted (Figure 3.14). For this reason, it is impossible for the sulcal basins boundaries to move to an unlabeled neighbor point with lower curvature value. If all boundaries regions grow up to the maximum curvature points then these boundaries meet at the top of the gyri.

The number of watershed regions must be equal to the number of sulcal basins.

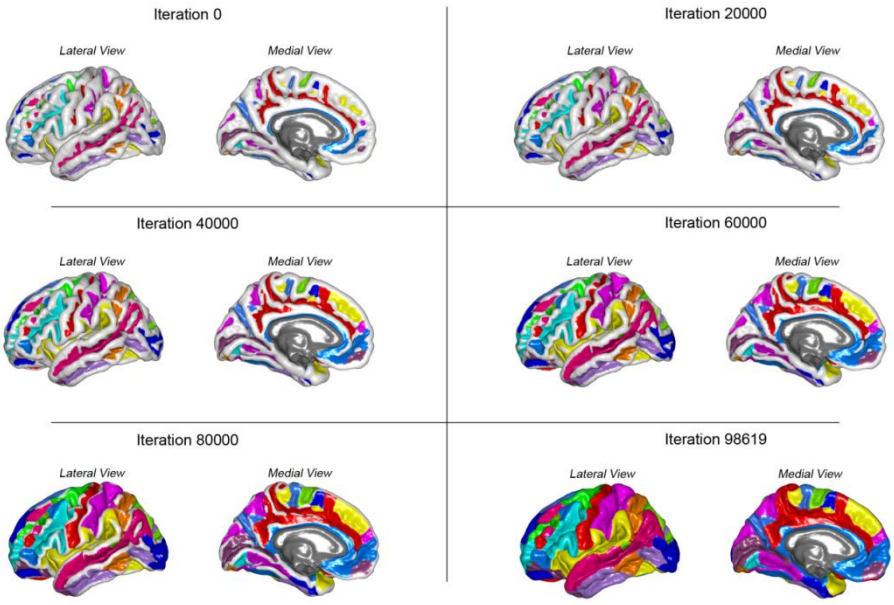

Figure 3.14: *Sulcal basins during different iterations of the watershed algorithm. The sulcal basins grow until a boundary between them is reached. The right inferior panel is the resulting labeled surface.*

Finally, based on this procedure, the gyral crowns are obtained simply by taking the boundaries between the regions created during the watershed parcellation (see Figure 3.15). As a side note it should be noted that, unlike the sulcal lines, the gyral crowns are continuous through the surface; so, in order to keep track of which gyral crown belongs to which watershed region, the labeling is maintained.

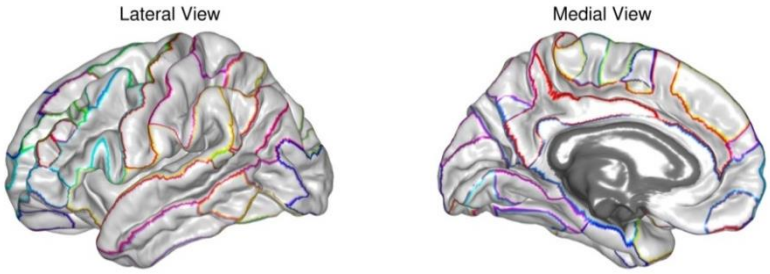

Figure 3.15: *Labeled gyral crowns obtained from curvature restricted watershed algorithm.*

3.6 Geodesic Path between Gyral Crown and Sulcal Line

At this point in the procedure, both the sulcal lines and the gyral crowns are combined into a single surface, in which the original labeling is maintained to ensure that a sulcal line is correctly situated with respect to its corresponding gyral crown. Since both lines and crowns were calculated from the same sulcal basins surface, the chances of a mismatching number of sulcal lines and gyral crowns are very low.

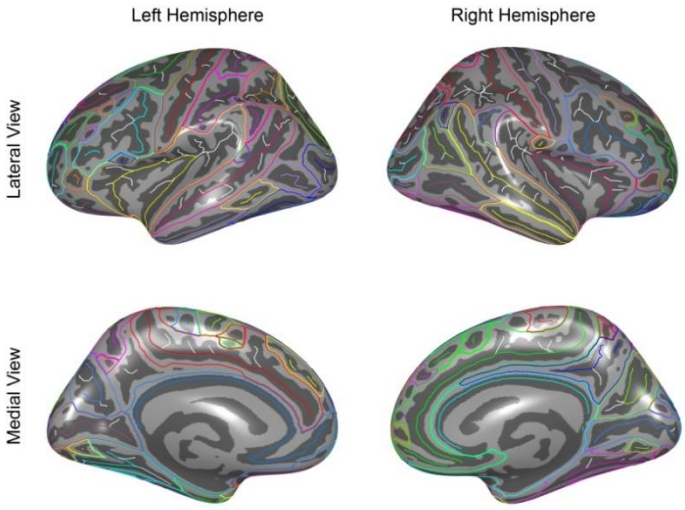

Figure 3.16: *Sulcal lines and gyral crowns for all watershed parcellated regions. White lines are sulci branches.*

For each of the watershed parcellation regions, the shortest geodesic paths between gyral crowns and sulcal lines points were calculated using Dijkstra's algorithm (Dijkstra 1959). In this case, the edges weights are the Euclidean distances between edges endpoints.

Out of all the paths available in one watershed region, (as many as points in the gyral crowns) the one selected to be used for the geodesic paths is the longest within that region, which is the *depth profile*. This selection is based on the importance of sulcal pits (the deepest part of the sulcal line) related to intelligence and neurodevelopment in human brains (Im et al. 2011), and also due to the fact that these pits are considered as deep sulcal landmarks (Auzias et al. 2015); since the depth profile will be the one communicating the gyral crown to the points in the sulcal pits, the geodesic profile obtained from this depth profile is more likely to be of scientific importance.

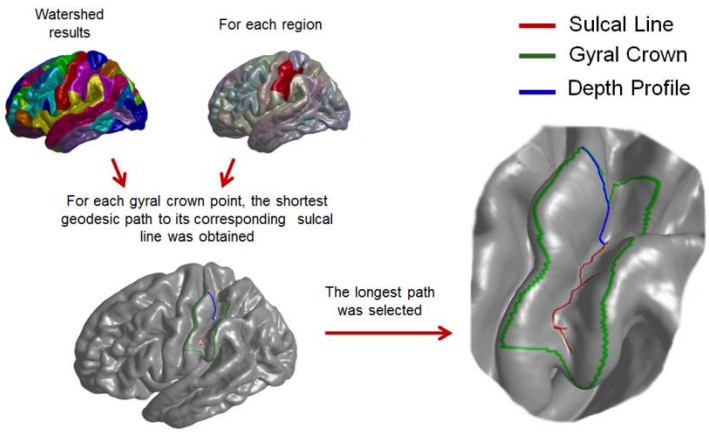

Figure 3.17*: Path between gyral crowns and sulcal lines points. Only, the longest depth path is selected for each watershed parcellated regions*.

3.7 Building the Morphometric Profile along the Depth Path

Finally, the generation of the geodesic profiles consists of plotting the values of the morphometric maps (depending on the property to be analyzed) along the points of the depth profile (see Figure 3.18).

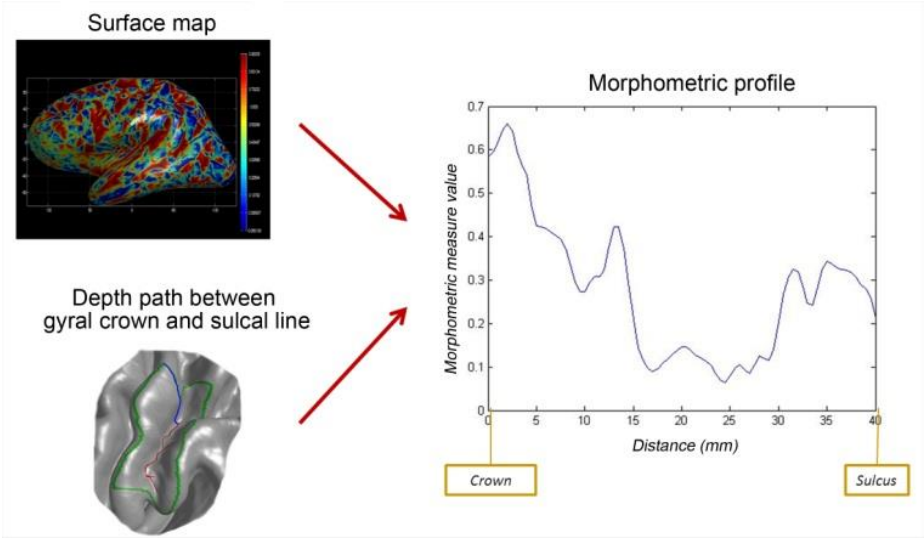

Figure 3.18: *A morphometric profile allows for observing the behavior of a morphometric measure (fractional anisotropy, in this example) along the path that connects the gyral crown and the sulcal line.*

Using the depth profiles, it is also possible to plot two properties from the surface maps one against the other across the profile; however, this plot's biological significance is yet to be researched.

In the case of cortical maps (cortical thickness, area and local gyrification index) obtained from the image processing step using FreeSurfer, the morphometric profiles building is straight forward because they are already *surface maps*. On the other hand, for DW-MRI scalar maps (fractional anisotropy, mean diffusivity and radial diffusivity), previous to constructing the morphometric profiles, an interpolation step must be performed in order to project the tridimensional data from the images onto the white surface.

The resulting *surface maps* show the corresponding quantitative measures in the cortex surface (Figure 3.19). For this work a spline interpolation was performed, but other interpolation approaches can be used (nearest neighbor, polynomial, etc.). The main advantage of spline interpolation is the high level of smoothness within the profile curve, and that if the function is a piecewise function there is a more controlled behavior within the interpolation.

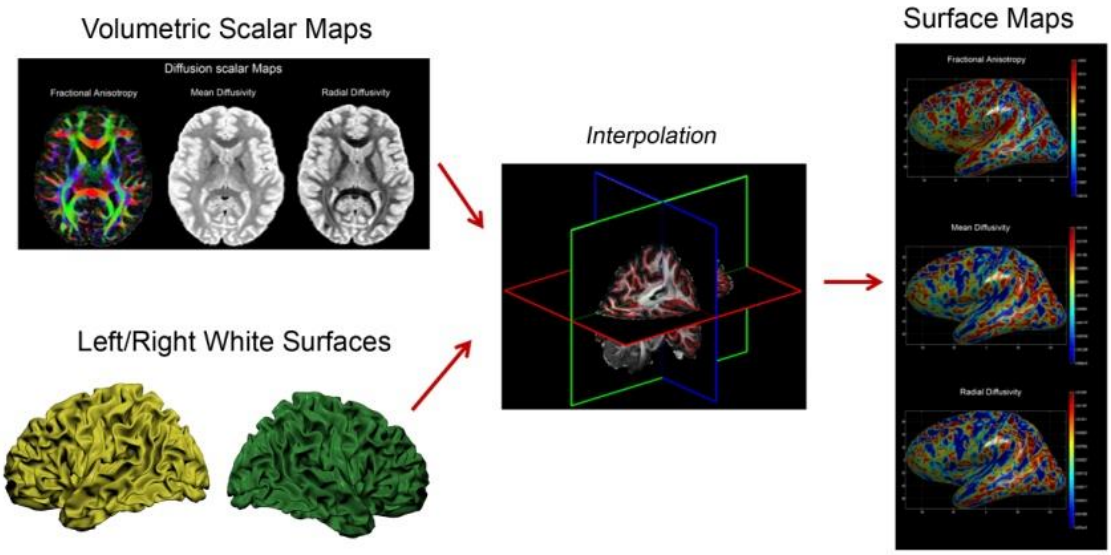

Figure 3.19: *Interpolation of the volumetric scalar maps (obtained from DW-MRI) into the white surface points yields surface maps of the diffusion scalar properties.*

The surface maps used correspond to those explained in Chapter 2.3; they are Cortical Thickness, Local Gyrification Index, Area, Fractional Anisotropy, Mean Diffusivity and Radial Diffusivity.

Chapter 4: Results and Discussion

The results presented in this chapter follow two objectives. First, the validation of the novel approaches developed throughout this work, mainly, the sulcal lines extraction algorithm. Next, the results stated as the main goal of this Project, which are composed by different applications that use morphometric profiles along the human brain cortex to study biomarkers and biological structural properties obtained from MRI and DW-MRI.

Method validation can only be performed for the sulcal lines extraction algorithm due to the fact that no comparison with prior work regarding the two other objectives of this work (the extraction of gyral crowns and the morphometric profiles along the sulcal depth path) was possible. Therefore, the accuracy of the gyral crown extraction and the morphometric profiles relies on visual inspection. Extraction of sulcal lines was validated by comparing the results with the ones produced by BrainVisa software, which is explained in (Le Troter et al. 2012) and briefly commented in Chapter 2.4.1. BrainVisa was chosen for validation because it is considered as one of the most reliable and widely used tools for extracting sulcal lines.

In the second section, three possible applications of the methodology are discussed:

- Plotting the profile of a morphometric measurement along the sulcal depth path
- Using the sulcal depth path as a region of interest (ROI) in order to assess the relationship between morphometric measurements within the ROI.
- Analyzing the correlation between morphometric measurements at each point along the geodesic sulcal depth path.

These applications may provide useful information for the discussion of neurodevelopmental research on the human brain cortex morphometry. However, neuroscientific discussion about this neurodevelopmental and morphometric theories are out of the scope of this work.

The validation and morphometric profiling was performed only for eight different sulcal basins, four per hemisphere, each basin pertaining to a different lobe (frontal, occipital, parietal and temporal).

4.1 Validation of Sulcal Lines Extraction

A statistical comparison was performed between the sulcal lines obtained with BrainVisa and the ones obtained with the proposed method. Two different statistical metrics were used. First the *Dice Similarity Index* (DSI), which yields a measure of the overlapping percentage between lines obtained by both methods. The second metric is the geodesic *Distance Between the extracted Lines* (DBL). It differs from the DSI analysis because it does not analyze the degree of coincidence between lines, but how close the lines are. In Figure 4.1, results from sulcal lines extraction using both methods are shown:

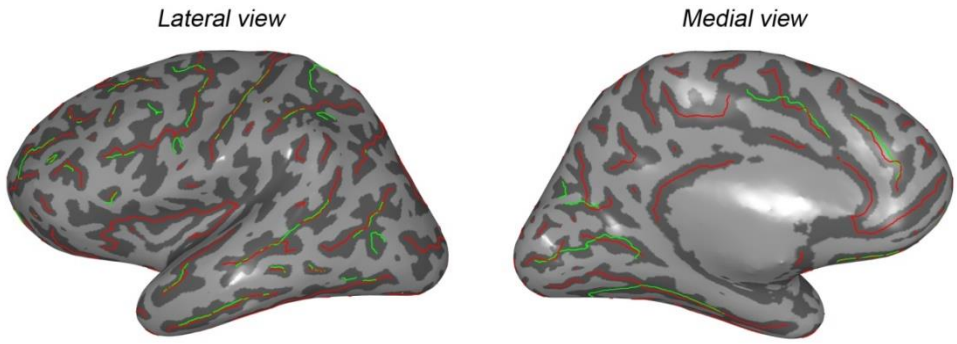

Figure 4.1: *Sulcal lines extracted by both methods on top of a curvature map.* ***Green****: Sulcal lines extracted from BrainVisa.* ***Red****: Sulcal extracted using the proposed methodology.*

4.1.1 Dice Similarity Index Results

The Dice similarity index is the most well-known statistical index to compare the similarity between sets and it can be defined by the following expression:

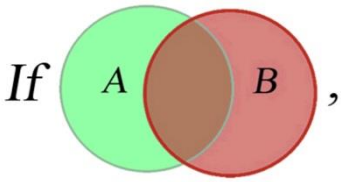

$$DSI(A,B) = \frac{2|A \cap B|}{|A| + |B|}$$

In this work, set A is composed by the lines obtained via BrainVisa and the set B is defined by the lines obtained from the proposed method. If both set of lines perfectly coincide over the surface then the DSI value will be 100 %. If both set of lines do not share any line point then the DSI value will be 0 %.

In the next figures (see Figure 4.2), DSI histograms, showing the number of coinciding lines inside each hemisphere for certain DSI levels, are presented. The

horizontal axis represents the Dice similarity index and the vertical axis is the total number of lines (considering the 165 subjects).

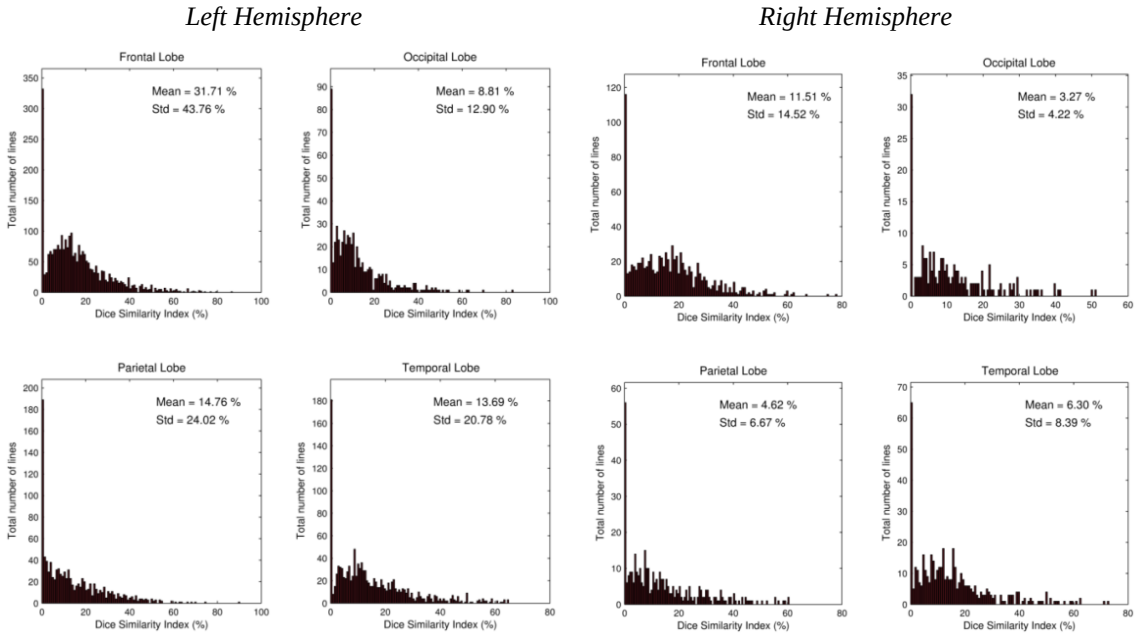

Figure 4.2: *DSI between sulcal lines obtained with BrainVisa and sulcal lines obtained with the proposed method.*

As it can be seen from the figures, the Dice similarity index appears to be relatively low. The frontal lobe values show a higher mean percentage of coincidence because it has a higher amount of gyri and sulci, so the number of sulcal lines is increased with respect to the other lobes. This anatomical feature increases the probability of coinciding points because there are more points from both extracted sulcal lines. On the other hand, the occipital lobe has a lower gyrification index compared to other lobes, and it is also the most difficult lobe to extract its surface. Since the quality of the surface influences its curvature values, which are used to calculate the sulcal lines, the mean percentage of coincidence between lines in the occipital lobe is lower than the rest because there are fewer sulcal lines with fewer coinciding point.

It must be noted that the cortical surfaces presents a very high spatial resolution (around 10^5 or 10^6 surface points). Thus, the probability of an exact overlapping between two points is very low. Due to this high resolution of the mesh, however, a different statistical analysis can be performed to study the distance between the extracted lines in both methods, which would evaluate the similarity of the results in a more significant way.

4.1.2 Distance Between Lines Results

The metric created to study the distance between the extracted sulcal lines from one method to the other is based on a similar measure found in (Le Troter et al. 2012). It will be referred in next discussions as distance between lines (DBL). This distance is a mean pairwise geodesic distance between sulcal lines extracted using both methodologies.

A histogram of the DBL is constructed for all the extracted lines of the 165 subjects (see Figure 4.3). The X axis represents the closest distance (in mm) between points from one method's lines and points from the other. The vertical axis represents the total number of points in the extracted sulcal lines.

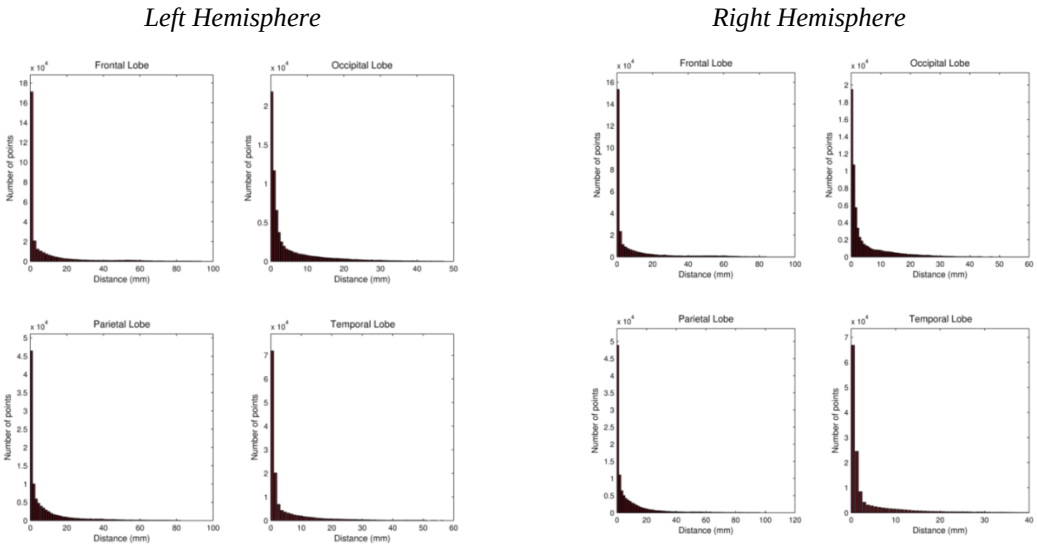

Figure 4.3: *DBL between sulcal lines obtained with BrainVisa and sulcal lines obtained with the proposed method.*

The information provided by these DBL histograms establishes that the distances between lines points are low enough to be considered as viable. In most of the cases, the vast majority of the points are in a close radius of 15 mm and the largest part of this majority is around 2 mm apart. Therefore, it can be safely stated that the proposed method is reliable compared to BrainVisa's because both lines are relatively close to each other.

4.1.3 Computation Time Comparison

Due to the long processing time, it is also important to compare both methods computation time, not only to see if the developed method is as fast as BrainVisa's but also to see if it runs faster, thus adding extra value to it. As it can be seen in the table,

the computation time was lower than BrainVisa's. The results on this table are an average of the individual computation time for each subject.

	Our Method	BrainVisa
Sucal Lines Extraction	6 min/subject	20 min/subject
Gyral Crowns Extraction	40 min/subject	N/A
Geodesic Profile	2 min/subject	N/A

4.1.4 Final Discussion about the Validation

With all the validation results shown, it is clearly seen that our method not only equals BrainVisa's performance in terms of accuracy and reliability, but it also improves on it by being faster and also adding the extraction of gyral crowns and geodesic depth paths. All previous results were calculated including only lines that were extracted by both methods. Future work should include a sensibility study about the total number of lines extracted by both methods because it appears that the proposed methodology is capable of obtaining a higher number of lines (see Figure 4.1).

4.2 Morphometric Profiles along the Human Brain Cortex

The main objective of this work is to extract the morphometric profiles of several diffusion and anatomical properties and use them to create plots showing different representations of the behavior of these properties across the sulcal depth of the cortex. In order to be able to compare and relate these profiles between different subjects or groups of subjects, it is necessary that they are represented in the same coordinate system. To guarantee spatial correspondence, a spatial normalization step must be applied, meaning by spatial normalization the spatial alignment of one or more images or surfaces to a common space (Collins et al. 1994).

In this case, surface maps normalization was performed throughout a surface-based registration method. In this step, the individual pial surfaces (both hemispheres) are mapped to a sphere and the curvature maps are employed for surface-based spatial normalization (Fischl et al. 1999). The 2D spherical coordinate of a vertex is adjusted so as to best match the curvature across subjects. Aligning the curvature aligns the folding patterns (i.e., gyri and sulci) (see Figure 4.4).

Surface-based spatial normalization causes that parts of the surface may be compressed or stretched in order to obtain the best match between curvature maps. The obtained spatial transformation is applied to each subject surface maps to re-map them into a common surface space. Once this step is performed, the characterization and comparison of morphometric profiles across subjects is possible.

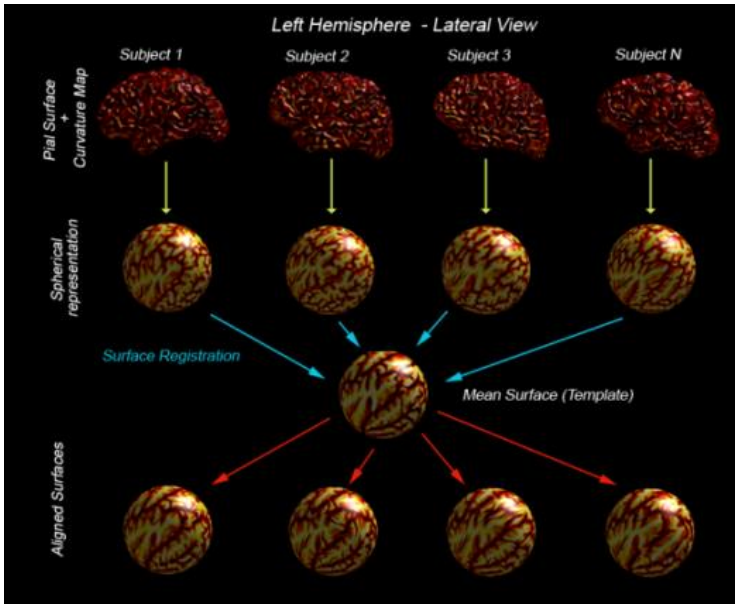

Figure 4.4: *Surface alignment and normalization strategy for cortical surfaces.*

Three possible applications of the extraction of morphometric profiles along the human brain cortex are presented below. It is important to note again that the biological significance and the neuroscientific interpretation of the following results are out of the scope of this Project.

4.2.1 Profiles versus Sulcal Depth

In this application, the plots of the profiles of six morphometric biomarkers along the sulcal depth path (distance from the gyral crown to the sulcal pit) are displayed. The biomarkers employed in this epigraph were previously described at Chapter 2.3.

Each of the plots that are shown below is an average profile over the 100 subjects for four different sulcal basins located at the left hemisphere (each basin pertaining to a different lobe: frontal, occipital, parietal and temporal) (see Figure 4.5). In these profile plots, the X-axis represents the distance between the gyral crown and

each point on the geodesic depth path and the Y-axis represents the value of the biomarker.

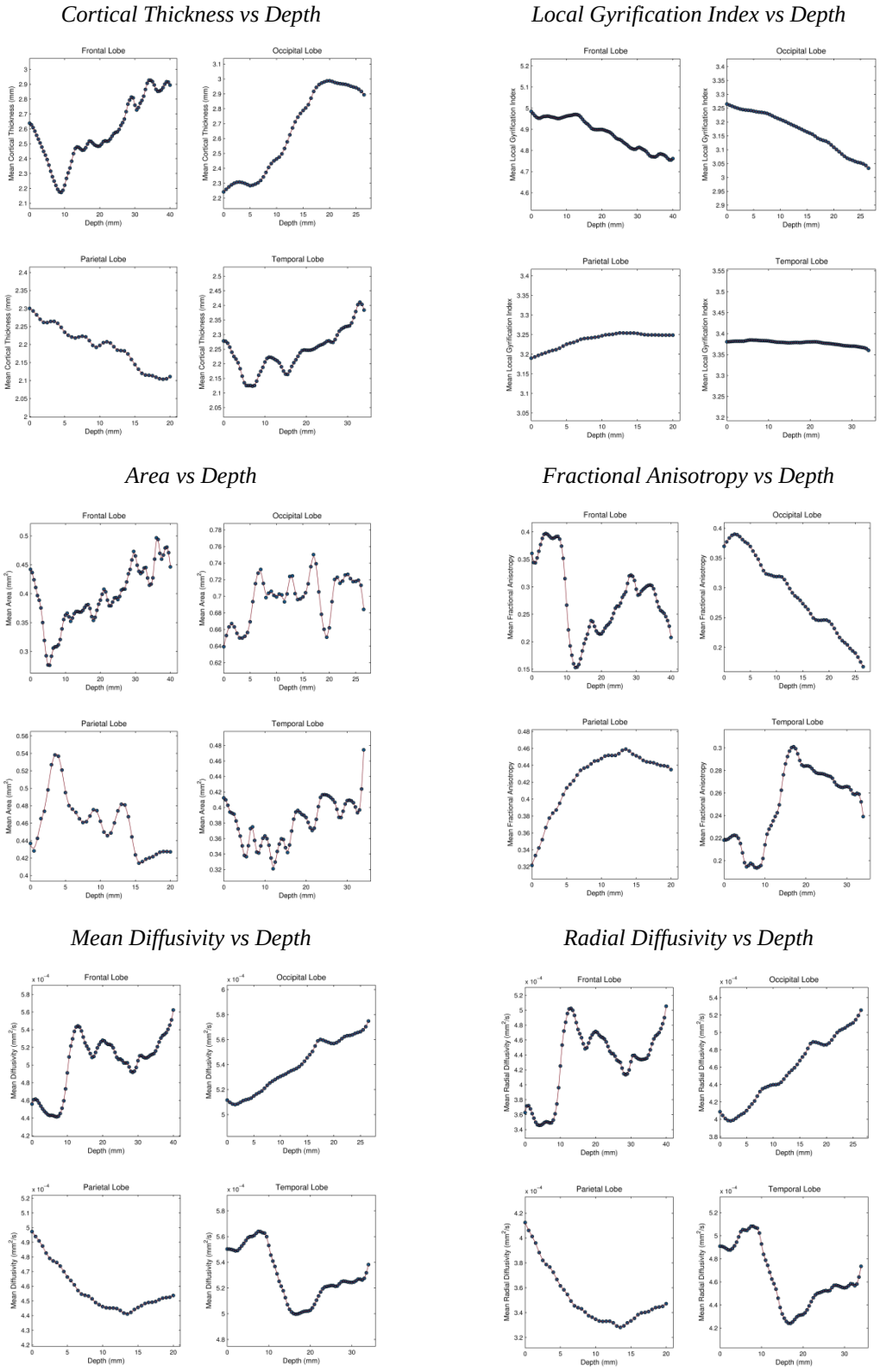

Figure 4.5: *Plots of cortical and white matter biomarkers versus depth along the morphometric profile.*

As it can be seen, the neurodevelopmental information that can be obtained from these profiles is huge. The tendency that all these properties follow along the depth profile, from the top of the gyral crown to the pit of the sulcal line, is clearly shown for all lobes. Further neuroscientific study can be vastly benefited from the usage of these tools.

4.2.2 Correlation between Morphometric Profiles

Another application of the morphometric profiles consists on the plotting of two morphometric biomarkers, one against the other, to see how the relationship between them changes within a region of interest (ROI). In this case, the ROI is the geodesic depth path, since the values for these biomarkers are extracted from the morphometric profiles.

Unlike the previous section, the biomarkers information presented in these plots is displayed for all subjects. In this case, each pair of coordinates (Y vs X) represents the values of two different morphometric measurements at the same point of the sulcal depth path. A regression line has been added to the plots to highlight a possible relationship between biomarkers.

Cortical Thickness vs Local Gyrification Index

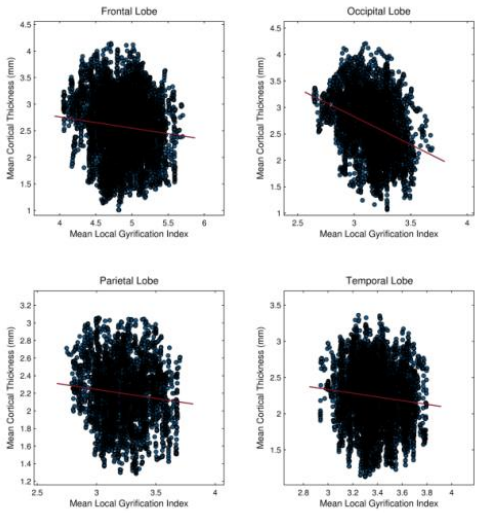

Cortical Thickness vs Fractional Anisotropy

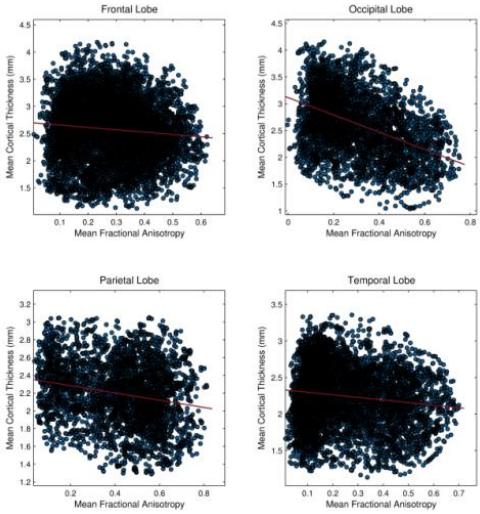

Mean Diffusivity vs Fractional Anisotropy *Local Gyrification Index vs Mean Diffusivity*

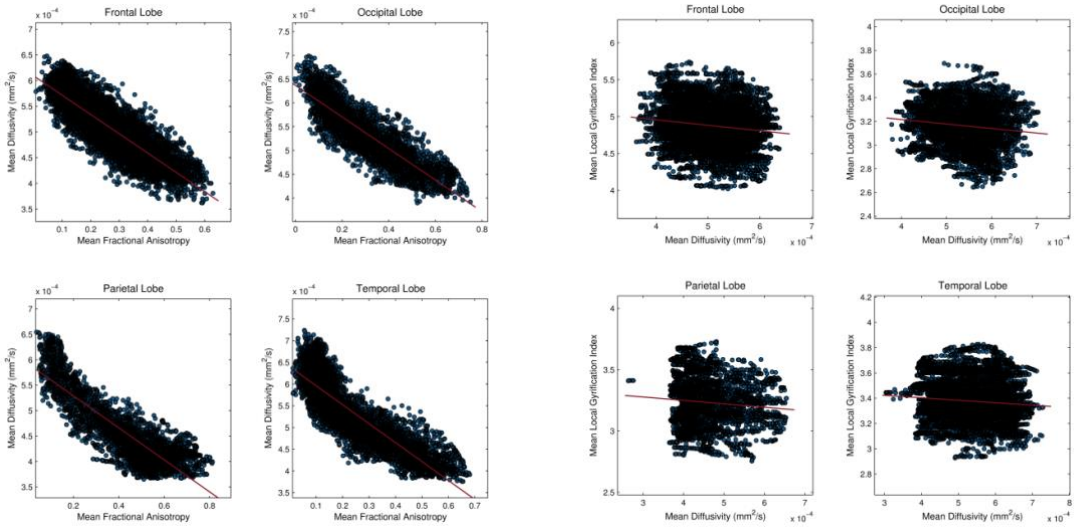

Figure 4.6: *Plots of the values of two biomarkers in a ROI defined by the morphometric profile.*

While many of the biological importance this kind of analysis may convey is yet to be researched, it is interesting to know that the tools to create these biomarker regression plots are already available.

4.2.3 Correlation versus Sulcal Depth

Finally, to study how the correlation of two biomarkers changes against the geodesic depth, a pointwise correlation analysis can be performed.

Afterwards, plotting the sulcal depth in the horizontal axis and the value of the correlation in the vertical yields a plot showing how the correlation between two randomly selected measurements changes across the profile.

In these plots, the Y-axis represents the correlation between two different biomarkers at a certain depth point and the X-axis represents the geodesic distance between that point and the gyral crown (sulcal depth path).

Correlation between CT and Area vs Depth

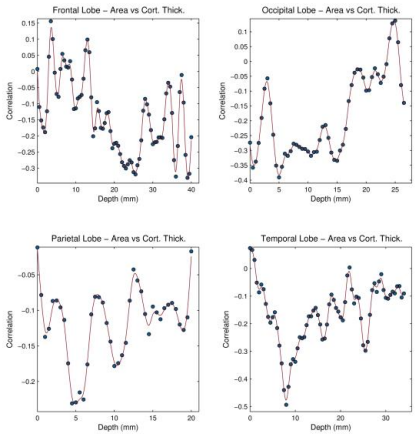

Correlation between MD and CT vs Depth

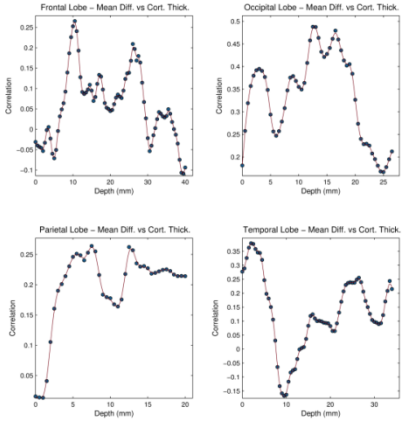

Correlation between FA and RD vs Depth

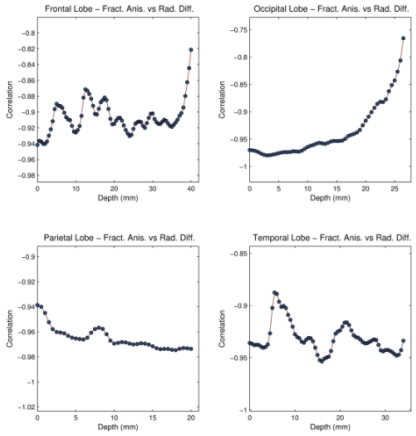

Correlation between FA and LGI vs Depth

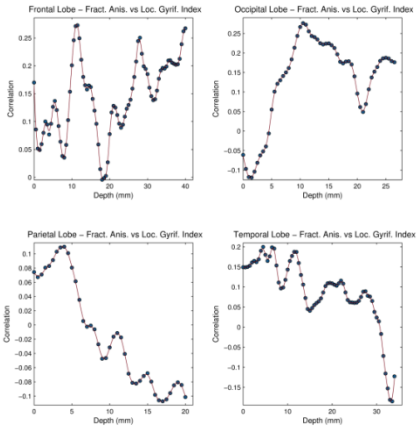

Figure 4.7: *Correlation plots between two biomarkers versus depth along the morphometric profile.*

The results that come out of the three applications answer the main objective and motivation of this work. At this point, it is possible not only to study the anatomical features at the top of the gyrus or at the sulcus fundus but how these biomarkers change across the depth path between gyral crowns and sulcal fundi.

Chapter 5: Conclusions and Future Work

5.1 Conclusions

The final conclusions of this Project answer to the objectives stated in Chapter 1.3. Therefore, it is concluded that:

1. Geodesic paths between gyral crowns and sulcal lines were obtained.
   a. Both the gyral crowns and the sulcal lines were extracted in a robust way, improving the methods already available in the literature.
   b. Geodesic depth paths connecting the gyral crowns with the sulcal lines were computed.
2. Morphometric profiles along the geodesic paths were computed.
   a. Cortical biomarkers (cortical thickness, area and local gyrification index) were calculated from T1W-MRI images.
   b. White matter biomarkers (fractional anisotropy, mean diffusivity and radial diffusivity) were calculated from DW-MRI images.
   c. Volumetric scalar maps containing biomarker values were projected onto the cortical surfaces.
   d. Biomarkers profiles across the geodesic paths were obtained.

5.2 Limitations

There are several limitations to the methodology and results presented in this report. Some of them must be addressed in the future work (see Chapter 5.3), while others are natural limitations to the work and are theorically impossible to overcome.

These are the most relevant limitations of this work:

1. The sulcal lines extraction algorithm has no *gold standard*. Therefore, the validation of the proposed algorithm is not 100% reliable, although the results against BrainVisa are good. Also, validation using other methods (like those presented in Chapter 2.4.1 or a manual labeling by an expert) could not be performed in this Project because of time limitations.
2. The gyral crowns extraction algorithm could not be validated since no other method available in the literature yielded satisfying results.

3. There is no neuroscientific interpretation of the applications developed. This interpretation is out of the scope of this Project due to its large body of information and vast potential.

5.3 Future Work

According to the limitations presented in the last epigraph, some future work is proposed:

- To consolidate the validation of the algorithms, a neuroscience expert could be approached to manually label the sulcal lines and the gyral crowns of some patients. The proposed methods for these processes would be much better studied if compared to the manual labeling than to BrainVisa (in the case of sulcal lines) or to any other available method (in the case of gyral crowns).
- To test the robustness of the procedures, the proposed methodology could be applied to poor quality images (the ones used in this Project had a high quality, see Chapter 3.1). The sensibility of the results could also be evaluated using these images.
- Many other applications of the morphometric profiles could be developed, since only three examples of possible applications are shown in this Project (see Chapter 4.2). For example, using each point of the profile a group comparison of all subjects could be performed, for one or more biomarkers.
- Other biomarkers may be implemented in the morphometric profiles, like myelin maps, for example, to see how the degree of myelization changes across the sulcal depth.
- Finally, the neuroscientific discussion of the results from the applications of these morphometric profiles is enormous. Many neurodevelopmental studies could be performed using these tools, either to aid in the premature detection or the monitoring and treatment of neurodegenerative diseases.

Related References

(2001). "Biomarkers and surrogate endpoints: preferred definitions and conceptual framework." Clin Pharmacol Ther **69**(3): 89-95.

Ashburner, J. and K. J. Friston (2000). "Voxel-based morphometry--the methods." Neuroimage **11**(6 Pt 1): 805-821.

Ashburner, J. and K. J. Friston (2005). "Unified segmentation." Neuroimage **26**(3): 839-851.

Auzias, G., L. Brun, et al. (2015). "Deep sulcal landmarks: Algorithmic and conceptual improvements in the definition and extraction of sulcal pits." Neuroimage **111**(Journal Article): 12-25.

Basser, P. J. (1995). "Inferring microstructural features and the physiological state of tissues from diffusion-weighted images." NMR Biomed **8**(7-8): 333-344.

Basser, P. J. (1995). "Inferring microstructural features and the physiological state of tissues from diffusion-weighted images." NMR in biomedicine **8**(7-8): 333.

Basser, P. J. (1997). "New histological and physiological stains derived from diffusion-tensor MR images." Ann N Y Acad Sci **820**: 123-138.

Basser, P. J., J. Mattiello, et al. (1994). "MR diffusion tensor spectroscopy and imaging." Biophys J **66**(1): 259-267.

Beaulieu, C. (2002). "The basis of anisotropic water diffusion in the nervous system - a technical review." NMR Biomed **15**(7-8): 435-455.

Brown, R. C., A. H. Lockwood, et al. (2005). "Neurodegenerative diseases: an overview of environmental risk factors." Environ Health Perspect **113**(9): 1250-1256.

Campero, A., P. Ajler, et al. (2014). "Brain sulci and gyri: a practical anatomical review." Journal of clinical neuroscience : official journal of the Neurosurgical Society of Australasia **21**(12): 2219-2225.

Clouchoux, C., D. Rivière, et al. (2010). "Model-driven parameterization of the cortical surface for localization and inter-subject matching." Neuroimage **50**(2): 552-566.

Collins, D. L., P. Neelin, et al. (1994). "Automatic 3D intersubject registration of MR volumetric data in standardized Talairach space." Journal of computer assisted tomography **18**(2): 192.

Cusack, R. (2005). "The Intraparietal Sulcus and Perceptual Organization." Journal of cognitive neuroscience **17**(4): 641-651.

Dale, A., B. Fischl, et al. (1999). "Cortical Surface-Based Analysis II: Inflation, Flattening, and a Surface-Based Coordinate System." Neuroimage **9**(2): 195-195.

Davatzikos, C. and N. Bryan (1996). "Using a deformable surface model to obtain a shape representation of the cortex." IEEE Trans Med Imaging. **15**(6): 785-795.

Davatzikos, C., A. Genc, et al. (2001). "Voxel-based morphometry using the RAVENS maps: methods and validation using simulated longitudinal atrophy." Neuroimage **14**(6): 1361-1369.

Delibasis, K. S., G. K. Matsopoulos, et al. (2001). "A novel and efficient implementation of the marching cubes algorithm." Comput Med Imaging Graph **25**(4): 343-352.

Dijkstra, E. W. (1959). "A note on two problems in connexion with graphs." Numerische Mathematik **1**(1): 269-271.

Durrleman, S., X. Pennec, et al. (2007). "Measuring brain variability via sulcal lines registration: a diffeomorphic approach." Med Image Comput Comput Assist Interv **10**(Pt 1): 675-682.

Essen, D. C. V. (1997). "A tension-based theory of morphogenesis and compact wiring in the central nervous system." Nature **385**(6614): 313-318.

Fischl, B., N. Rajendran, et al. (2008). "Cortical folding patterns and predicting cytoarchitecture." Cerebral cortex (New York, N.Y.: 1991) **18**(8): 1973.

Fischl, B., D. H. Salat, et al. (2002). "Whole brain segmentation: automated labeling of neuroanatomical structures in the human brain." Neuron **33**(3): 341-355.

Fischl, B., M. I. Sereno, et al. (1999). "Cortical surface-based analysis. II: Inflation, flattening, and a surface-based coordinate system." Neuroimage. **9**(2): 195-207.

Gülgen, F. and T. Gökgöz (2004). "Automatic Extraction of Terrain Skeleton Lines from Digital Elevation Models." International Archives of Photogrammetry, Remote Sensing and Spatial Information Sciences 35(B3).(Journal Article).

Hurd, M. D., P. Martorell, et al. (2013). "Monetary costs of dementia in the United States." N Engl J Med **368**(14): 1326-1334.

Im, K., Y. Y. Choi, et al. (2011). "The relationship between the presence of sulcal pits and intelligence in human brains." Neuroimage **55**(4): 1490-1496.

Joshi, A. A., D. Pantazis, et al. (2010). "Sulcal set optimization for cortical surface registration." Neuroimage **50**(3): 950-959.

Kao, C. Y., M. Hofer, et al. (2007). "A geometric method for automatic extraction of sulcal fundi." IEEE Trans Med Imaging **26**(4): 530-540.

Khaneja, N., M. I. Miller, et al. (1998). "Dynamic programming generation of curves on brain surfaces." IEEE Transactions on Pattern Analysis and Machine Intelligence **20**(11): 1260-1265.

Kim, J. S., V. Singh, et al. (2005). "Automated 3-D extraction and evaluation of the inner and outer cortical surfaces using a Laplacian map and partial volume effect classification." Neuroimage. **27**(1): 210-221.

Koutsouleris, N., C. Gaser, et al. (2012). "Multivariate patterns of brain-cognition associations relating to vulnerability and clinical outcome in the at-risk mental states for psychosis." Hum Brain Mapp **33**(9): 2104-2124.

Kruskal, J. B. (1956). "On the shortest spanning subtree of a graph and the traveling salesman problem." In Proceedings of the American Mathematical Society **7**: 48-50.

Le Bihan, D. (1995). "Diffusion, perfusion and functional magnetic resonance imaging." J Mal Vasc **20**(3): 203-214.

Le Goualher, G., E. Procyk, et al. (1999). "Automated extraction and variability analysis of sulcal neuroanatomy." IEEE Trans Med Imaging **18**(3): 206-217.

Le Troter, A., G. Auzias, et al. (2012). "Automatic sulcal line extraction on cortical surfaces using geodesic path density maps." Neuroimage **61**(4): 941-949.

Li, G., L. Guo, et al. (2010). "An automated pipeline for cortical sulcal fundi extraction." Medical image analysis **14**(3): 343-359.

Liang, Z.-P. and P. C. Lauterbur (2000). Principles of magnetic resonance imaging: signal processing perspective. Bellingham (Washington); New York, SPIE Optical Engineering Press.

Lohmann, G. (1998). "Extracting line representations of sulcal and gyral patterns in MR images of the human brain." IEEE Transactions on Medical Imaging **17**(6): 1040-1048.

Lohmann, G., F. Kruggel, et al. (1997). Automatic detection of sulcal bottom lines in MR images of the human brain. BERLIN, SPRINGER-VERLAG BERLIN. **1230:** 369-374.

Lui, L. M., Y. Wang, et al. (2006). Automatic landmark tracking applied to optimize brain conformal mapping, IEEE.

Melbourne, A., G. S. Kendall, et al. (2014). "Preterm birth affects the developmental synergy between cortical folding and cortical connectivity observed on multimodal MRI." Neuroimage **89**(Journal Article): 23-34.

Narr, K. L., T. Sharma, et al. (2000). "Cortical surface asymmetries and sulcal shape variability in schizophrenia." Schizophrenia research **41**(1): 123-124.

Ono, M., S. Kubik, et al. (1990). Atlas of the cerebral sulci, Thieme.

Paus, T., N. Otaky, et al. (1996). "In vivo morphometry of the intrasulcal gray matter in the human cingulate, paracingulate, and superior-rostral sulci: Hemispheric asymmetries,

gender differences and probability maps." Journal of Comparative Neurology **376**(4): 664-673.

Prim, R. (1957). "Shortest connection networks and some generalizations." Bell System Technical Journal **36**: 1389-1401.

Prince, M. (2013). "The Global Prevalence of Dementia: A Systematic Review and Metaanalysis." Alzheimer's and Dementia **9**: 63-75.

Rettmann, M. E., X. Han, et al. (2002). "Automated Sulcal Segmentation Using Watersheds on the Cortical Surface." Neuroimage **15**(2): 329-344.

Schaer, M., M. B. Cuadra, et al. (2008). "A surface-based approach to quantify local cortical gyrification." IEEE Trans Med Imaging **27**(2): 161-170.

Shattuck, D. W., A. A. Joshi, et al. (2009). "Semi-automated method for delineation of landmarks on models of the cerebral cortex." Journal of neuroscience methods **178**(2): 385-392.

Smith, S. M., M. Jenkinson, et al. (2004). "Advances in functional and structural MR image analysis and implementation as FSL." Neuroimage **23 Suppl 1**: S208-219.

Thirion, J. P. and A. Gourdon (1992). "The 3D marching lines algorithm and its application to crest lines extraction." Research Report **1672**(Journal Article).

Thirion, J. P. and A. Gourdon (1993). "The Marching Lines Algortihm: new results and proofs." (Journal Article).

Thompson, P. M., J. Moussai, et al. (1998). "Cortical variability and asymmetry in normal aging and Alzheimer's disease." Cereb Cortex **8**(6): 492-509.

Van Essen, D. C., K. Ugurbil, et al. (2012). "The Human Connectome Project: a data acquisition perspective." Neuroimage **62**(4): 2222-2231.

Yaçargil, M. G. (1996). "Microneurosurgery." (Journal Article).